DSCAM Localization and Function at the Mouse Cone Synapse

Gabriel Belem de Andrade,[1,2] Samuel S. Long,[3] Harrison Fleming,[4] Wei Li,[5] and Peter G. Fuerst[1,6]*

[1]Department of Biological Sciences, University of Idaho, Moscow, Idaho 83844
[2]Ministry of Education of Brazil, CAPES Foundation, Brasília-DF 70.040-020, Brazil
[3]Department of Electrical Engineering and Computer Sciences, Washington State University, Pullman, Washington 99164
[4]Department of Biology, Brigham Young University–Idaho, Rexburg, Idaho 83460
[5]Unit on Retinal Neurophysiology, National Eye Institute, U.S. National Institutes of Health, Bethesda, Maryland 20892
[6]WWAMI Medical Education Program, University of Washington School of Medicine, Moscow, Idaho 83844

ABSTRACT

The Down syndrome cell adhesion molecule (DSCAM) is required for regulation of cell number, soma spacing, and cell type–specific dendrite avoidance in many types of retinal ganglion and amacrine cells. In this study we assay the organization of cells making up the outer plexiform layer of the retina in the absence of *Dscam*. Some types of OFF bipolar cells, type 3b and type 4 bipolar cells, had defects in dendrite arborization in the *Dscam* mutant retina, whereas other cell types appeared similar to wild type. The cone synapses that these cells project their dendrites to were intact, as visualized by electron microscopy, and had a distribution and density that was not significantly different from that of wild type. The spacing of type 3b bipolar cell dendrites was further analyzed by Voronoi domain analysis, density recovery profiling (DRP) analysis, and nearest neighbor analysis. Spacing was found to be significantly different when wild-type and mutant type 3b bipolar cell dendrites were compared. Defects in arborization of these bipolar cells could not be attributed to the disorganization of inner plexiform layer cells that occurs in the *Dscam* mutant retina or an increase in cell number, as they arborized when *Dscam* was targeted in retinal ganglion cells only or in the bax null retina. Localization of DSCAM was assayed and the protein was localized near to cone synapses in mouse, macaque, and ground squirrel retinas. DSCAM protein was detected in several types of bipolar cells, including type 3b and type 4 bipolar cells. J. Comp. Neurol. 522:2609–2633, 2014.

© 2014 Wiley Periodicals, Inc.

INDEXING TERMS: synapse; development; adhesion; pedicle; spherule; rod; cone; horizontal cell; connectome; mosaic; differential adhesion hypothesis

---

The first synapses in the photopic visual transduction pathway are those between cone photoreceptors and bipolar and horizontal cells. A single cone axon terminal, or pedicle, makes a series of complex synapses in which the dendrites of bipolar and horizontal cells are organized into multiple distinct signaling hubs. Each of these hubs at a given cone pedicle is composed of the invaginating dendrites of cone bipolar and horizontal cells, facing a presynaptic ribbon, whereas additional bipolar cell dendrite tips make flat contacts arrayed on the lateral edges of the invaginating ON bipolar and horizontal cell dendrites (Boycott and Hopkins, 1991; Haverkamp et al., 2000; Hopkins and Boycott, 1992). Mechanisms underpinning the developmental organization of this structure are largely unexplored. In this study we assay the role of the Down syndrome cell

adhesion molecule (DSCAM) in the organization of the cells making the multiple synapses that compose the cone synapse.

Vertebrate Dscams differ from *Drosophila* Dscam1 in that they lack the extensive alternative splicing that occurs in the insect gene (Schmucker et al., 2000). Remarkably, despite this difference, many of the protein's reported functions are conserved between

vertebrates and fly (Schmucker and Chen, 2009). For example, Dscams in both fly and vertebrates have been implicated in axon guidance, self-avoidance, and organization of synaptic pairing and targeting (Fuerst et al., 2008; Liu et al., 2009; Ly et al., 2008; Matthews et al., 2007; Millard et al., 2010; Neves et al., 2004; Schmucker et al., 2000; Wang et al., 2002; Yamagata and Sanes, 2008). In the retina, Dscams have been implicated in both a passive form of self-avoidance, early in development, and in synaptic lamination and coupling through adhesion (Fuerst et al., 2008, 2009; Yamagata and Sanes, 2008). Functional studies of DSCAM in the retinal outer plexiform layer have not been performed, whereas *Dscaml1* is required for organization of the cells making up the mouse rod circuit, suggesting that *Dscam* may function in organization of cone circuits (Fuerst et al., 2009). Unlike the inner plexiform layer of the retina, in which the synapses are very small and difficult to individually image, the large cone synapses offer the opportunity not only to assay the development of the structure itself, but to also study the function of DSCAM in synapse formation and maintenance.

In this study we characterize the localization and function of DSCAM at the mammalian cone synapse. We find that DSCAM is localized on the postsynaptic face of the mouse, squirrel, and macaque cone synapse. Defects in the arborization of some OFF populations of cone bipolar cells were observed in the absence of *Dscam*. These defects were not the result of increases in cell number or disorganization of cells contributing to the inner plexiform layer of the retina. This study therefore identifies DSCAM as an essential organizer of the dendritic fields of some populations of OFF bipolar cells.

MATERIALS AND METHODS
Animals
Mouse strains. The following mouse strains were used in this study
$Dscam^{2J}$ mice
$Dscam^{2J}$ mice contain a 4-bp insertion that disrupts the *Dscam* gene. A detectable DSCAM protein product is not made by these mice (Fuerst et al., 2010; Schramm et al., 2012). $Dscam^{2J}$ mice were maintained on a C3H/HeJ inbred background in which the *Pde6b* (rd1) gene is wild type. Wild-type siblings were used as controls in these studies.

$Dscam^{FD}$ and $Dscam^{F}$ mice
The *Dscam* floxed allele was generated by flanking the exon encoding the *Dscam* transmembrane domain with

loxP sites, allowing for tissue-specific targeting of the *Dscam* gene (Fuerst et al., 2012). The $Dscam^{FD}$ allele was generated by targeting the floxed exon in the germline. No significant morphological differences have been detected when comparing the $Dscam^{FD}$ allele with the $Dscam^{2J}$ allele or when comparing the $Dscam^{F}$ allele with wild type. Both alleles were backcrossed to the rd1 corrected C3H/HeJ genetic background that the $Dscam^{2J}$ allele is carried on for 10 generations, after which they were maintained by intercrossing siblings.

Brn3b-Cre mice
The Brn3b-Cre transgene is a knockin allele that expresses Cre recombinase in most retinal ganglion cells (Fuerst et al., 2012). It had been backcrossed to the rd1 corrected C3H/HeJ genetic background for four generations at the time of study.

Bax mutant mice
The Bax null strain is maintained on a C57Bl/6J genetic background.

Mouse care and housing
All protocols were performed in accordance with the University of Idaho Institutional Animal Care and Use Committee. Mice were fed ad libitum under a 12-hour light/dark cycle.

Ground squirrel
Ground squirrels were housed and eyes were obtained as previously described (Chen and Li, 2012).

Macaque
Eyes were obtained from a single 11-year-old female macaque that was euthanized for other reasons at the Davis primate center.

Mouse genotyping
Mice were genotyped by polymerase chain reaction (PCR) as previously described (Fuerst et al., 2008, 2009, 2010, 2012). Tail or toe tip biopsies were prepared for genotyping by boiling biopsies in 75 µl 25 µM sodium hydroxide and 0.2 µM EDTA for 15 minutes. Samples were neutralized with an equal volume of Tris Cl, pH 5.0. DNA was added to OneTaq Hot Start 2X Master Mix with standard buffer, along with primers and water to dilute the PCR mixture to 1X concentration (New England Biolabs, Ipswich, MA).

Tissue preparation
Mice were anesthetized and perfused with phosphate-buffered saline, pH 7.4 (PBS) prior to enucleation. Eyes from all three species were hemisected

<div align="center">

TABLE 1.

Primary Antibodies

</div>

Antigen	Immunogen	Manufacturer and details	Dilution
NK3R	Synthetic peptide at the c-terminus of rat NK-3 (SFISSPYTSVDEYS)	Novus Biologicals, Littleton CO, cat. no. 300-102, rabbit polyclonal	1:2,000
Recoverin	Recombinant human recoverin	Millipore, Billerica, MA, cat. no. AB5585, rabbit polyclonal	1:2,000
HCN4	Amino acids 119–155 of human HCN4 (HGHLHDSAEERRLIAEGDASPGEDRTPPGLAAEPERP)	Alomone, Jerusalem, Israel, cat. no. APC-052, rabbit polyclonal	1:500
PKARIIβ	Amino acids 1–418 (full length) of human protein kinase A, regulatory subunit IIβ	BD Biosciences, Franklin Lakes, NJ, cat. no. P54720, mouse monoclonal IgG1	1:1,000
Calsenilin	Recombinant human calsenilin	Upstate Biotechnology, Lake Placid, NY, cat. no. clone 40A5, mouse monoclonal IgG1	1,1,000
Syt2	1–5-day-old zebrafish embryo	Zebrafish International Resource Center, Eugene, OR, cat. no. Znp-1, mouse monoclonal IgG2A	1,500
Go-α	Purified Go-α from bovine brain	Millipore, cat. no. MAB3073, mouse monoclonal IgG1	1:2,000
PKCα	An epitope mapping between amino acids 645 and672 at the C-terminus of protein kinase C α of human origin (IANIDQSDFEGFSYVNPQFVHPILQSAV)	Santa Cruz Biotechnology, Santa Cruz CA, cat. no. SC-8393, mouse monoclonal IgG1	1:2,000
β-Dystroglycan	C-terminal peptide β-dystroglycan (KNMTPYRSPPPYVPP)	Developmental Studies Hybridoma Bank, Iowa City, IA, cat. no. Mandag 2, mouse monoclonal IgG1	1:1,000
Cone arrestin	Synthetic peptide: EEFMQHNSQTQS	Millipore, cat. no. AB15282, rabbit polyclonal.	1:5,000
GS	Sheep glutamine synthetase(amino acids 1–373)	BD Transduction Laboratories, Franklin Lakes, NJ, cat. no. 610517, mouse monoclonal IgG2A	1:2,000
Calbindin D28K	Purified rat calbindin D-28	Swant, Bellinzona, Switzerland, cat. no. CB-38a, rabbit polyclonal	1:1,000
DSCAM	Mouse myeloma cell line NS0-derived recombinant human DSCAM long isoform	R&D Systems, Minneapolis, MN, cat. no. MAB36661, mouse monoclonal IgG2B	1:25
DSCAM	Mouse myeloma cell line NS0-derived recombinant human DSCAM long isoform	R&D Systems, cat. no. AF3666, goat polyclonal	1:100
Bassoon	Fusion protein amino acids 738–1075 of ground squirrel bassoon	Custom-made courtesy of Wei Li (Covance, Princeton, NJ), rabbit polyclonal	1:100
PSD95	Fusion protein amino acids 77–299 (PDZ domains 1 and 2) ofhuman PSD-95	UC Davis NeuroMab Facility, Davis, CA, cat. no. 75-028	1:1,000
ChAT	Human placental cholineacetyltransferase	Millipore, cat. no. AB144P, goat polyclonal	1:500
Brn3A	Amino acids 1–109 of Brn-3a of mouse origin	Santa Cruz Biotechnology, cat. no. SC-8429, mouse monoclonal IgG1	1:200
Disabled (Dab1)	GST-mouse Dab1 fusion protein corresponding to residues 107–243	Generous gift of Brian Howell, rabbit polyclonal	1:500
bNOS	Synthetic peptide corresponding to the C-terminal fragment of nNOS of rat brain origin (amino acids 1409–1429 with N-terminal added lysine: EDAGVFISRLRDDNRYHEDIF)	Sigma, St. Louis, MO, cat. no. N7280, rabbit polyclonal	1:10,000
Chx10	A peptide encompassing the amino acids 44–61 of human CHX10 (PPSSHPRAALDGLAPGHL)	Santa Cruz Biotechnology, cat. no. sc-21690, goat polyclonal	1:200

in PBS and immediately fixed in paraformaldehyde (PFA) under the following conditions: ground squirrel and macaque eyes were fixed in 4% PFA for 50 minutes on ice. Mouse eyes were fixed in 4% PFA for 50 minutes on ice (DSCAM staining) or 4% PFA for 30 minutes at room temperature (all other staining). Tissue was sunk in 30% sucrose overnight prior to freezing. Tissue was then immersed in Tissue-Tek optimal cutting temperature media (Sakura Finetek, Torrance, CA) and rapidly frozen by holding the tissue above the liquid phase of liquid nitrogen. Sections were cut at 10 μm onto charged slides.

Antibody characterization

See Table 1 for a list of all antibodies used, the dilution they were used at and the source of these reagents.

NK3R

The NK3R antibody used in this study is specific to the NK-3 receptor. Specificity was verified by the localization

of immunohistochemical staining as well as by preabsorption studies with NK-3 peptide, which eliminates staining (manufacturer's website) (Burke et al., 2006). NK3R has previously been characterized as a marker for type 1 and 2 cone bipolar cells, and the staining pattern we observed in this study is consistent with what has been reported in previous studies (Haverkamp et al., 2003).

Recoverin

The recoverin antibody labels a single band of 26 kDa by western blot analysis of protein extracted from human retinoblastoma Y79 cells (Wiechmann, 1996). Recoverin is expressed by bipolar cells in a number of species, including mouse, in which it labels type 2 cone bipolar cells, and the staining observed in this study is consistent with what has been previously reported (Haverkamp et al., 2003; Milam et al., 1993; Wikler et al., 1998).

HCN4

Western blot analysis using the polyclonal HCN4 antibody detects a dark band of approximately 130 kDa in extracts of rat brain membrane, compared with a predicted protein size of 129 kDa. This band and several fainter bands were not detected after preincubation with the antigen (manufacturer's website). HCN4 has been shown to be expressed by type 3 (later reclassified as type 3a) bipolar cells, and the morphology and stratification of the cells visualized in this study matched what has been previously observed (Muller et al., 2003).

PKARIIβ

The protein kinase A regulatory subunit IIβ (PKARIIβ) antibody recognizes a single band of 53 kDa by western blot analysis of protein extracted from human endothelial cells, close to the predicted size of the protein, 46 kDa (manufacturer's website). This antibody has previously been shown to label type 3b bipolar cells, and the staining we observed in this study is consistent with these results (Mataruga et al., 2007).

Calsenilin

The 40A5 antibody to calsenilin has previously been shown to label type 4 cone bipolar cells (Haverkamp et al., 2008). The specificity of the 40A5 monoclonal antibody used in Haverkamp et al. (2008) was demonstrated to be specific by performing western blot analysis, in which a single band, the same size as recombinant human calsenilin, was detected in retina protein extracts, and this band was absent when the antibody was preabsorbed with calsenilin antigen (Haverkamp et al., 2008).

Syt2

The specificity of Syt2 immunoreactivity was demonstrated by western blot analysis, in which a single 60-kDa band was detected in lysates of zebrafish embryos or mouse cerebellum but not liver. Syt2 immunoreactivity has previously been described in the soma, axons, and dendrites of type 2 bipolar cells and type 6 cone bipolar cell axons (Fox and Sanes, 2007; Wässle et al., 2009). Staining observed in this study matched what has previously been described in the mouse retina.

Go-α

Specificity of the Go-α antibody was verified by western blot analysis of Go-α and related proteins expressed in bacteria, in which a single band between 39 and 42 kDa is detected, consistent with the protein's predicted size of 40 kDA (manufacturer's website). Localization of Go-α to ON bipolar cells in the mouse retina has been previously described, and the localization observed in this study was consistent with these findings (Haverkamp and Wässle, 2000).

PKCα

Protein kinase C α (PKCα) specificity was confirmed by western blot analysis, in which a dark band between the 91 and 42 kDa markers was detected in Hela cell protein extracts treated with phorbol 12-myristate 13-acetate (PMA), compared with the predicted molecular weight of the protein, 77 kDa (manufacturer's website). PKCα is widely used as a marker for rod bipolar cells, and the morphology of the stained cells that we observed was similar to what many others have reported.

β-Dystroglycan

Specificity of the Mandag2 antibody was confirmed by staining retina tissue from a mouse lacking the region of the protein in which the epitope is located (courtesy of Dr. Kevin Campbell and Rolf Turk, University of Iowa). Staining of blood vessels and rod and cone synapses by this antibody was absent in mice lacking the epitope-containing region, whereas staining in the inner plexiform layer was still present, indicating that the inner plexiform staining is nonspecific (Fig. 1A,B).

Cone arrestin

This antibody recognized a single band in protein lysates made from mouse retina, located between 37 and 50 kDa markers, consistent with the protein's predicted size of 42 kDa, (manufacturer's website). Specificity was also confirmed by costaining with peanut agglutinin (PNA) and by the characteristic morphology of the cone pedicle (Nasonkin et al., 2011).
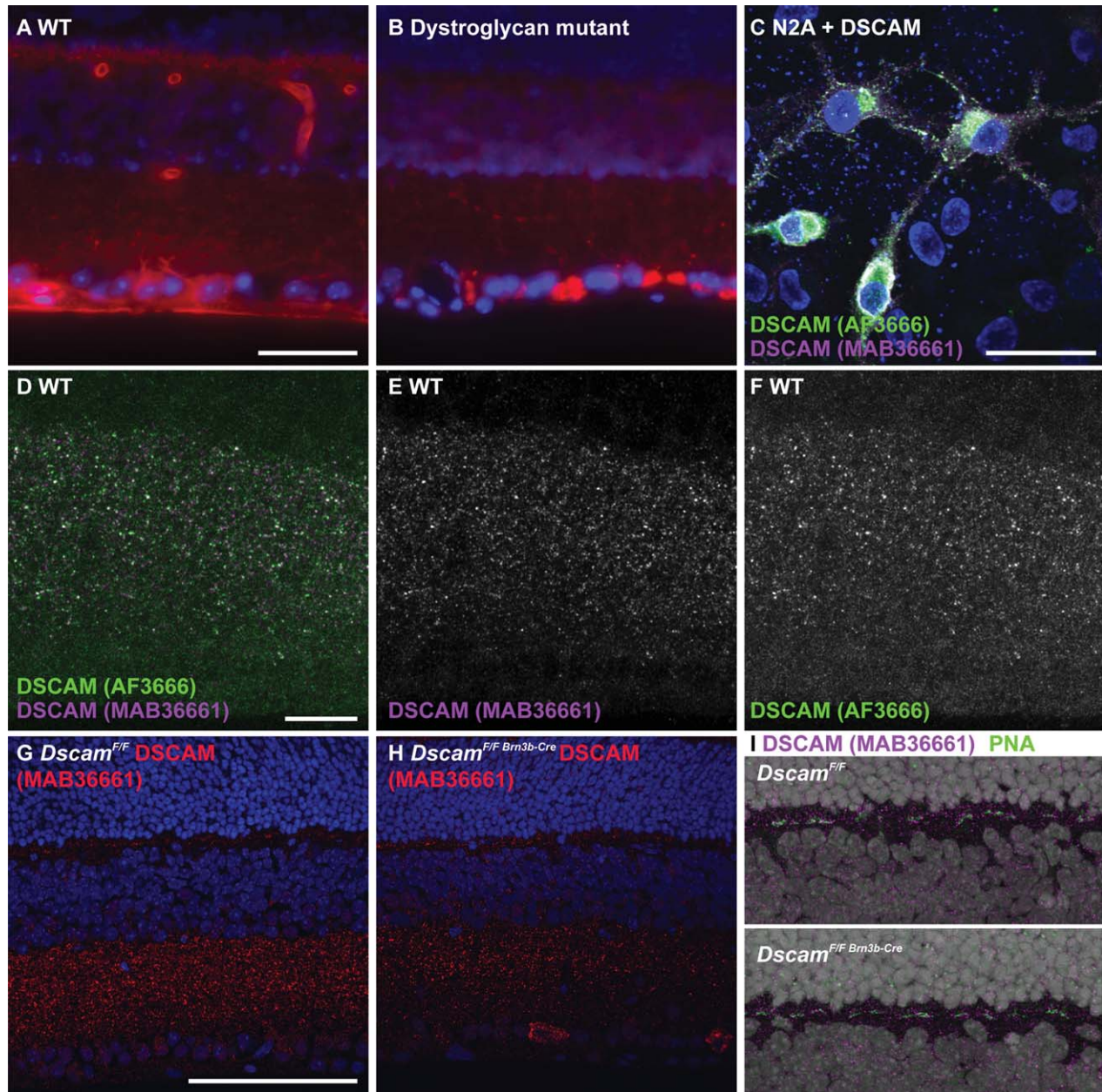
Figure 1. Antibody and strain characterization. **A,B:** Sections of retina from wild-type and dystroglycan mutant mice were stained with the Mandag2 antibody. Based on the differences between the two genotypes, blood vessel and photoreceptor synapse staining by the antibody is specific, whereas staining of ganglion cell axons, dendrites, and cell bodies is not. **C:** Neuro2A cells transfected with a full-length *Dscam* expression construct were immunostained with two different DSCAM antibodies. The two antibodies stained the same structures, with no staining present in untransfected cells. **D–F:** Section of wild-type retina stained with AF3666 and MAB36661 antibodies. The two antibodies stain a largely overlapping set of puncta in the mouse inner nuclear layer. **G–I:** Sections of *Dscam^F/F* or *Dscam^F/F Brn3b-Cre* retina stained with antibodies to DSCAM. A reduction in DSCAM immunoreactivity is observed in the inner plexiform layer, and cells in the retinal ganglion cell layer accumulate DSCAM protein in their soma in the presence of Brn-3b Cre. DSCAM protein is observed adjacent to the cone synapse in both genotypes. Scale bar = 50 μm in A (applies to A,B); 20 μm in C; 20 μm in D (applies to D–F,I); 100 μm in G (applies to G,H).

GS

Specificity of this antibody was demonstrated by western blot analysis in which a single band of 45 kDa was detected in protein extracted from rat brain, the predicted size of the protein (manufacturer's website). The antibody has also been used in retina and has a staining pattern consistent with specific labeling of Müller glia (Puller and Haverkamp, 2011).

Calbindin

This antibody stains a single band of 28 kDA, the expected size of the protein, in western blot analysis of brain extracts from a variety of species including mouse. The D28K antibody is widely used in retinal research, and the staining pattern observed in this study was very similar to what has been previously reported.

DSCAM antibodies

DSCAM antibodies were first assayed on neuro-2a cells transfected with a plasmid encoding the full-length *Dscam* gene under control of the CAG promoter. Both mouse and goat antibodies colabeled protein in the membrane and endomembrane systems of transfected cells (Fig. 1C).

DSCAM (goat)

The polyclonal DSCAM antibody AF3666 stains a band of 220 kDa by western blot analysis of mouse retina, cortex, and cerebellum. Staining is absent in protein extracts generated from *Dscam*[2J] mice or reduced in size when detecting protein extracts made from *Dscam*[FD] mice, in which the DSCAM transmembrane domain is absent (Schramm et al., 2012). Staining in tissue sections showed overlap with the MAB36661 antibody, although some additional nonspecific staining was present (Fig. 1D–F).

DSCAM (mouse)

The staining pattern of the DSCAM MAB36661 antibody overlaps with the AF3666 antibody, and its staining is eliminated in sections of *Dscam*[2J] retina, in which no protein product is detected by western blot analysis. Furthermore, DSCAM immunoreactivity was detected in retinal cell types in which *Dscam* mRNA has been detected by in situ hybridization and was absent in those in which mRNA was not detected. The epitope of this antibody was deletion-mapped to the first four Ig repeats of the DSCAM protein (data not shown). The DSCAM MAB36661 antibody did not detect DSCAM by western blot analysis, suggesting that the epitope is sensitive to denaturation.

Bassoon

The ground squirrel bassoon antiserum recognized two expected bands of around 400 kDa on western blots of ground squirrel retina and stained a pattern of cellular morphology and distribution in the mouse retina that is identical with previous reports of mouse bassoon antiserum (Dick et al., 2003).

PSD95

Specificity of postsynaptic density protein 95 (PSD95) antibody was determined by performing western blot analysis using brain tissue generated from wild-type and knockout mice (manufacturer's website). Tissue from wild-type mice had bands between 95 and 110 kDA, consistent with the phosphorylation-dependent size of the protein, whereas no bands were detected in tissue extracts made from mutant mice. The immunoreactivity observed in this study matched the localization pattern of PSD95 in the retina.

ChAT

The choline acetyltransferase (ChAT) antibody recognizes bands of 70–74 kDa by western blot analysis of protein extract of mouse brain, consistent with the protein's predicted size of 68–70 kDa (manufacturer's website). The retina has a population of cholinergic amacrine cells that stratify in the ON and OFF lamina of the inner plexiform layer. The antibody used in this study recognized this population of cells and is widely used to assay this cell population in the retina and to demarcate the inner plexiform layer, including in mouse; the staining pattern we observed is similar to what many others have reported (Pérez De Sevilla Muller et al., 2007).

Brn3A

This antibody recognizes a single band of 47 kDa in ND7 cells transfected with Brn3A by western blot analysis, the predicted size of the Brn3A protein. Staining was observed in the appropriate layer of the retina and in many Brn3b-positive (and therefore retinal ganglion) cells, but cells in the *Brn3b* null retinal ganglion cell layer were also recognized, indicating that it is not cross-reacting with this homologous transcription factor (data not shown).

Disabled

The Dab1 antibody has been used extensively to label type AII amacrine cells, which make a characteristic bistratified projection of their neurite arbors. Specificity of this antibody has been demonstrated by the absence of staining in knockout mice (Kuo et al., 2005).

bNOS

The neuronal nitric oxide synthase (bNOS) antibody is used to label a mixed population of amacrine cells, which was observed in this study. Antibody specificity was assayed by western blot of brain lysate, in which the immunizing peptide blocked detection of a band between 150 and 160 kDa, consistent with the

protein's predicted size of 150–160 kDa (manufacturer's website).

Chx10

Chx10 is expressed by bipolar cells and is used as a marker for this cell type in the retina (Burmeister et al., 1996). The antibody used in this study labels a single band slightly larger than the 43-kDa marker band in western blot analysis of eye extract, compared with the predicted protein size of 39.4 kDa (manufacturer's website). The expected localization pattern was observed in this and previous studies (Martinez-Navarrete et al., 2008).

Cre pattern verification

Brn3b-Cre activity was previously observed in retinal ganglion cells, but actual activity depends on the sensitivity of the target of recombination. For example, activation of the highly sensitive Cre reporter ai14 can be observed in retinal ganglion cells as well as off target cells such as horizontal cells, whereas recombination and activation of less sensitive reporters such as *Gt(ROSA)26Sortm4*[(ACTB-tdTomato,-EGFP)Luo/J] are not observed in any cells of the retina (data not shown). Brn3b-Cre activity was therefore verified by staining for DSCAM protein after targeting the *Dscam* transmembrane domain in the *Dscam*[F/F] mouse, which results in accumulation of residual DSCAM protein in the endomembrane system of the cell. Induction of recombination targeting the *Dscam* conditional allele using Brn3b-Cre resulted in a reduction of DSCAM immunoreactivity in the inner plexiform layer and accumulation of DSCAM protein in cells in the retinal ganglion cell layer, whereas DSCAM protein was still observed in the outer plexiform layer, consistent with Cre activity being targeted to retinal ganglion cells and also consistent with the phenotypes reported here (Fig. 1G–I).

Antibody staining

Tissue was blocked in a blocking solution composed of PBS, 5% normal donkey serum, and 0.1% Triton X-100 (for staining sections) or 0.4% Triton X-100 (for staining whole retinas) for 30 minutes (sections) or between 2 hours and overnight (whole retinas). Antibodies were diluted in blocking solution according to the concentrations listed in Table 1. Sections were incubated overnight at 4°C, after which they were washed three times for 10 minutes in PBS. Secondary antibodies (Jackson ImmunoResearch, West Grove, PA, at 1:2,000), peanut lectin (Molecular Probes, Eugene, OR, at 1:2,000 dilution of manufacturer's recommended reconstitution volume) and the nuclear stain Draq5 (Cell Signaling Technology, Danvers, MA, at 1:500) were diluted in blocking solution and incubated for 2 hours at room temperature. Following secondary incubation, sections were washed three times for 10 minutes in PBS. If 4,6-diamidino-2-phenylindole (DAPI) was used to label nuclei, the reagent was incorporated into the second wash at a dilution of 1:50,000 of a 1 mg/ml stock. Following washes, coverslips were applied to the slides using 80% glycerol as a mounting medium. Whole retinas were stained in a similar manner except that both primary and secondary incubations lasted for 2–4 days and were performed at 4°C. Washes were carried out for 1 hour each.

Fluorescent microscopy

Sections and whole retina were imaged using either an Olympus spinning disk (DSU) confocal microscope or Olympus Fluoview confocal microscope. Images were cropped and rotated using Adobe Photoshop software. Any changes to brightness or contrast were made across entire images.

Electron microscopy

Electron microscopy was performed as previously described (Fuerst et al., 2009). Briefly, retinas were fixed in buffered 2% glutaraldehyde and 2% formaldehyde overnight and then rinsed in PBS. Retinas were rinsed 3 times for at least 5 minutes in 0.1 M cacodylate buffer, followed by fixation using 4% osmium tetroxide overnight. After three further rinses in 0.1 M cacodylate buffer (5 minutes each), dehydration was performed by rinses in increasingly concentrated ethanol. Embedding was performed by first rinsing tissue twice in propylene oxide (10 minutes each), followed by a rinse in a 50:50 mix by volume of propylene oxide and Spurr's resin, three long rinses in Spurr's resin (at least 10 hours each), and curing overnight. Samples were sectioned using a Reichert ultramicrotome. Sections were stained in 4% uranyl acetate with potassium permanganate for 12 minutes, rinsed with distilled deionized water, and dried (either overnight or for 1 hour under a heat lamp). Sections were further stained with lead acetate for 8 minutes, briefly rinsed with 0.1 M NaOH, rinsed with distilled deionized water, and dried (overnight or for 1 hour under a heat lamp). Samples were imaged using either a Phillips CM200 200KV TEM equipped with a Gatan digital camera system and LaB6 cathode, or an FEI T20 200KV TEM.

Imaging for spatial analysis
Cone pedicles

Four wild-type and four *Dscam*[2J] retinas were stained with cone arrestin and PNA and imaged. Four peripheral and four central 213-μm confocal stacks were collected

from each retina. Peripheral stacks were collected within 213 μm of the edge of the retina (i.e., one field of view on this instrument), whereas central stacks were collected within 213 μm of the optic nerve. Stacks were projected and the center of each pedicle was marked for Voronoi domain analysis.

Type 3b bipolar cells

Four wild-type and four $Dscam^{2J}$ retinas were imaged. Four 213-μm confocal stacks were collected from each retina midway between the optic nerve and the edge of the retina. Confocal stacks were opened in FIJI, and the most distal portion of the dendrite (referred to in this article as the dendrite bulb) before projection of distal dendrites to the cone pedicles was marked.

Voronoi domain analysis

Voronoi analysis was performed with Ka-me Voronoi image analyzer software (Khiripet et al., 2012). Each cone pedicle or dendrite bulb was marked, and an image of the Voronoi domains was exported along with the area of each domain. The coefficient of variation was calculated for each of the 16 images per genotype/location (cone pedicles: wild-type central, wild-type peripheral, mutant central, and mutant peripheral; or type 3b dendrite bulbs: wild type versus mutant) and used to perform a Student's t-test.

Density recovery profile analysis

Density recovery profile (DRP) analysis was performed using WinDRP 1.6.4 (http://wvad.mpimf-heidelberg.mpg.de/abteilungen/biomedizinischeOptik/software/WinDRP/index.html). Images were imported as BMP files, and the location of each dendrite bulb was marked. The cell diameter was set to 3 μm, the annulus width was set at 5 μm, and cells (dendrite bulbs) within 15 annuli were counted. The soma correction was not used (the first annulus bin is sometimes discarded because two cells cannot occupy the same space). This was not performed because we would be able to measure dendrite bulbs in close proximity to each other. The number of cells in each bin was averaged for each genotype and to calculate an average bin density. The packing indexes of each genotype were used to compare wild-type and mutant genotypes with a Student's t-test.

Nearest neighbor analysis

Nearest neighbor analysis was performed using the same software as that used for DRP analysis. The regularity index of each test is given and was used to compare the distribution with random simulations or across genotypes using a Student's t-test.

Tissue culture and transfection

Neuro-2a cells were obtained from American Type Culture Collection (Rockville, MD) and maintained in Dulbecco's modified Eagles medium (DMEM) supplemented with 10% fetal bovine serum, glutamine, and penicillin/streptomycin antibiotics. A plasmid carrying full-length Dscam under control of the CAG promoter was transfected into cells grown on poly-l-lysine–coated coverslips using the FuGENE 6 reagent (Promega, Madison, WI) at a ratio of 1 μg DNA to 3 μl FuGENE reagent (Schramm et al., 2012). Cells were cultured for 24 hours and then collected and fixed in 4% PFA for 5 minutes. Cells were stained using the same procedure used for retina sections.

RESULTS

The Dscam gene is required for normal regulation of cell number, dendrite arborization, and spacing of multiple amacrine and ganglion cell types (Fuerst et al., 2008, 2009; Keeley et al., 2012). The Dscam homologue Dscaml1 is required for organization of cells making up the mouse rod circuit: rods, rod bipolar cells, and AII amacrine cells (Fuerst et al., 2009). The organization of the outer plexiform layer was assayed to determine whether Dscam influences the organization of the outer plexiform layer, particularly the cone synapse. To this end the organization of multiple bipolar cell types, horizontal cells, cones, cone synapses, Müller glia, and rod synapses were imaged in retina sections of wild-type and $Dscam^{2J}$ mice; the latter do not make a detectable DSCAM protein. The markers used encompass five types of OFF bipolar cells in the mouse retina and two markers of ON bipolar cells, in addition to PNA, which labels the invaginating processes of ON bipolar cells (Koike et al., 2010). Most bipolar cell types had an organization that appeared similar in wild-type and $Dscam^{2J}$ retinas (Figs. 2, 3). Two types of OFF bipolar cells, type 3b (Fig. 2M–T) and type 4 bipolar cells (Fig. 3A–H), appeared to have clumped dendrites, reminiscent of the self-avoidance defect observed in Dscam null amacrine and retinal ganglion cells. Markers of other cell types associated with the cone synapse were used to assay the organization of cones, horizontal cells, Müller glia, and rod synapses (Fig. 4). The organization of these cell types appeared similar in wild-type and $Dscam^{2J}$ retinas.

Arborization defects in cell types contributing to the cone synapse suggested that Dscam might be required for normal development of the cone synapse. Electron microscopy was performed to determine whether the ultrastructure of the cone pedicle was intact in the $Dscam^{2J}$ retina. Ribbon synapses were observed in both the wild-type and $Dscam^{2J}$ retina, organized around the
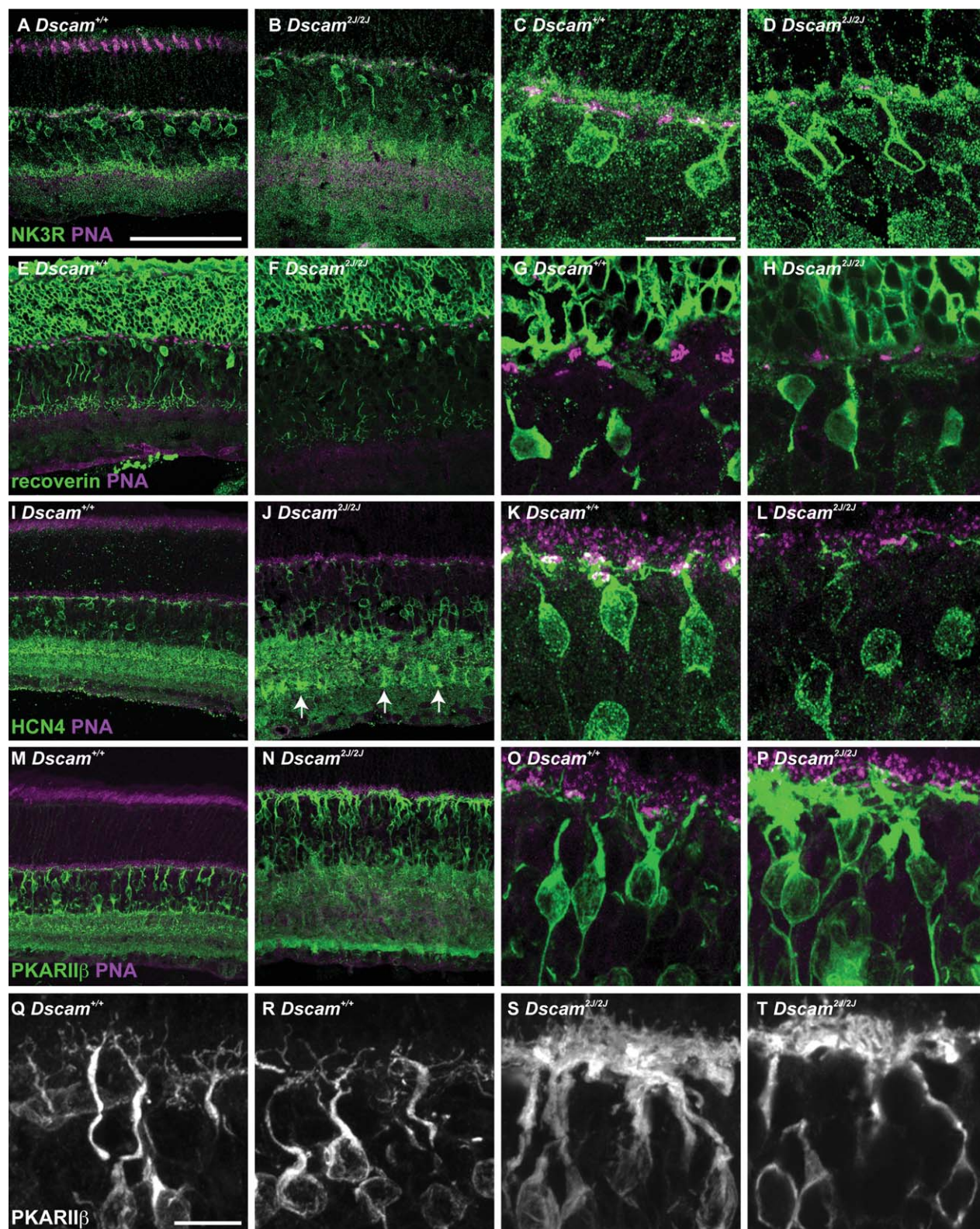
Figure 2. Axon and dendrite arborization of bipolar cells in the wild-type and *Dscam* loss of function retina. **A–D:** Sections of adult (>P42) wild-type and *Dscam*[2J/2J] retina were stained with antibodies to NK3R to label type 1 and type 2 cone bipolar cells, and PNA (*n* = 4 retinas). Differences when comparing wild-type and *Dscam* loss of function retina were not detected. **E,F:** Sections of adult (>P42) wild-type and *Dscam*[2J/2J] retinas were stained with antibodies to recoverin to label type 2 cone bipolar cells and rods, and PNA (*n* = 4 retinas). Differences when comparing wild-type and *Dscam* loss of function retina were not detected. **I–L:** Sections of adult (>P42) wild-type and *Dscam*[2J/2J] retinas were stained with HCN4 to label type 3a cone bipolar cells and PNA (*n* = 4 retinas). Lamination of HCN4-positive neurites in the ON half of the inner plexiform layer are longer in the *Dscam*[2J/2J] retina compared with wild-type controls (I vs. J; arrow). No differences were detected in the outer plexiform layer. **M–T:** Sections of adult (>P42) wild-type and *Dscam*[2J/2J] retinas were stained with antibodies to PKARIIβ to label type 3b cone bipolar cells and PNA (N > 4 retinas). PKARIIβ-immunopositive bipolar cells have clumped dendrite arbors proximal to cone pedicles, compared with wild type (P,S,T: mutant vs. O,Q,R: wild type). Scale bar = 100 μm in A (applies to A,B,E,F,I,J,M, N); 20 μm in C (applies to C,D,G,H,K,L,O,P); 10 μm in Q (applies to Q–T).
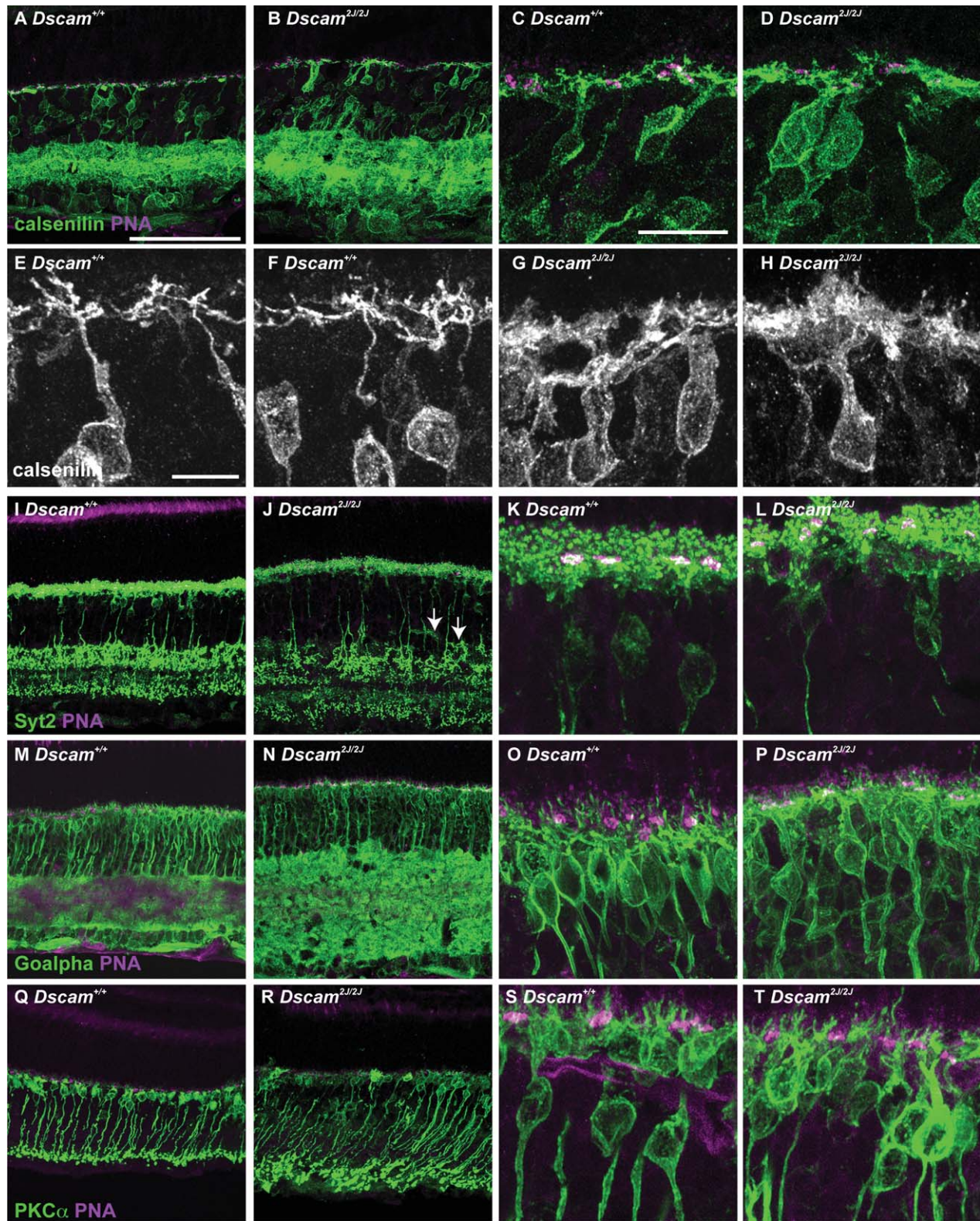
Figure 3. Axon and dendrite arborization of bipolar cells in the wild-type and *Dscam* loss of function retina. **A–H:** Sections of adult (>P42) wild-type and *Dscam²ᴶ/²ᴶ* retinas were stained with antibodies to calsenilin to label type 3b cone bipolar cells, and PNA (N > 4 retinas). Calsenilin-immunopositive bipolar cells have clumped dendritic arbors proximal to cone pedicles, compared with wild type (D,G,H: mutant vs. C,E,F: wild type). **I–L:** Sections of adult (>P42) wild-type and *Dscam²ᴶ/²ᴶ* retinas were stained with antibodies to Syt2 to label type 2 and type 6 cone bipolar cells, and PNA (*n* = 4 retinas). The terminals of some Syt2-positive bipolar cells terminated in the inner nuclear layer (arrows). Differences when comparing the outer plexiform layer of wild-type and *Dscam²ᴶ* retinas were not detected. **M–P:** Sections of adult (>P42) wild-type and *Dscam²ᴶ/²ᴶ* retinas were stained with antibodies to Go-α to label ON bipolar cells, and PNA (*n* = 4 retinas). Differences when comparing wild-type and *Dscam* loss of function retinas were not detected. **Q-T:** Sections of adult (>P42) wild-type and *Dscam²ᴶ/²ᴶ* retinas were stained with antibodies to PKCα to label rod bipolar cells, and PNA (*n* = 4 retinas). Differences when comparing wild-type and *Dscam* loss of function retinas were not detected. Scale bar = 100 μm in A (applies to A,B,I,J,M,N,Q,R); 20 μm in C (applies to C,D,K,L,O,P,S,T); 10 μm in E (applies to E–H).
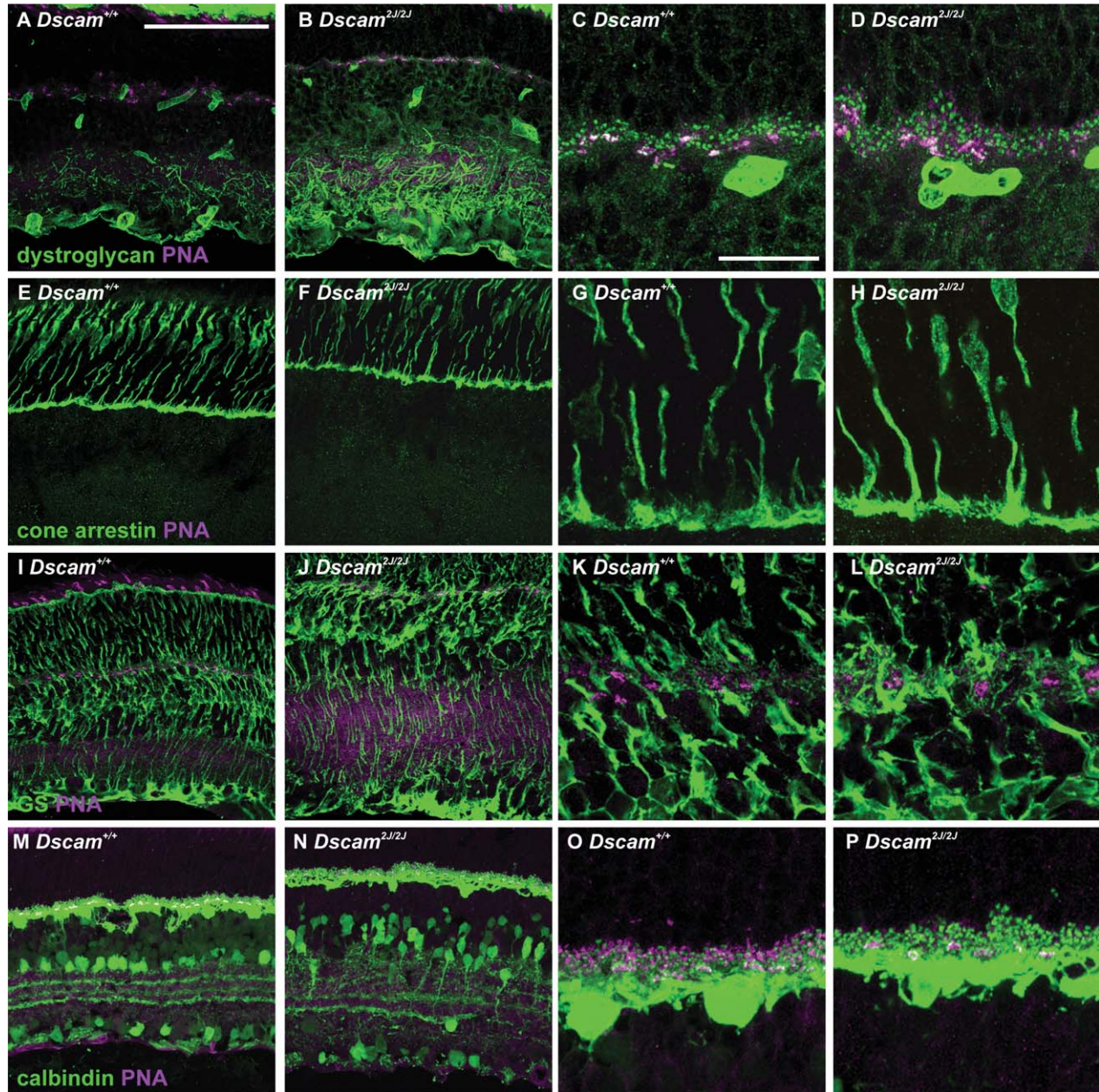
Figure 4. Organization of rod synapses, cone pedicles, Müller glia, and horizontal cells in the wild-type and *Dscam* loss of function retina. **A–D:** Sections of adult (>P42) wild-type and *Dscam*$^{2J/2J}$ retinas were stained with antibodies to dystroglycan to label rod and cone synapses, and PNA ($n = 4$ retinas). Differences when comparing wild-type and *Dscam* loss of function retinas were not detected. **E–H:** Sections of adult (>P42) wild-type and *Dscam*$^{2J/2J}$ retinas were stained with antibodies to cone arrestin to label cone cells, and PNA ($n = 4$ retinas). Differences when comparing wild-type and *Dscam* loss of function retinas were not detected. **I–L:** Sections of adult (>P42) wild-type and *Dscam*$^{2J/2J}$ retina were stained with antibodies to GS to label Müller glia, and PNA ($n = 4$ retinas). Differences when comparing wild-type and *Dscam* loss of function retina were not detected. **M–P:** Sections of adult (>P42) wild-type and *Dscam*$^{2J/2J}$ retina were stained with antibodies to calbindin to label horizontal cells, and PNA ($n = 4$ retinas). Disorganization of calbindin-positive amacrine cells was observed in the *Dscam* mutant retina. Differences when comparing horizontal cells in wild-type and *Dscam* loss of function retinas were not detected. Scale bar = 100 μm in A (applies to A,B,E,F,I,J,M,N); 20 μm in C (applies to C,D,G,H,K,L,O,P).

processes of invaginating bipolar and horizontal cells (Fig. 5). Cone pedicles were labeled to determine whether *Dscam* is required for their spatial organization. The organization of cone pedicles appeared similar in wild-type and *Dscam*^{2J} retinas, and telodendria were observed to project from the pedicles of both wild-type and *Dscam*^{2J} pedicles (Fig. 6A,B).

Voronoi domain analysis was performed to test whether there was a significant difference in the space occupied by wild-type and *Dscam*^{2J} pedicles. Voronoi
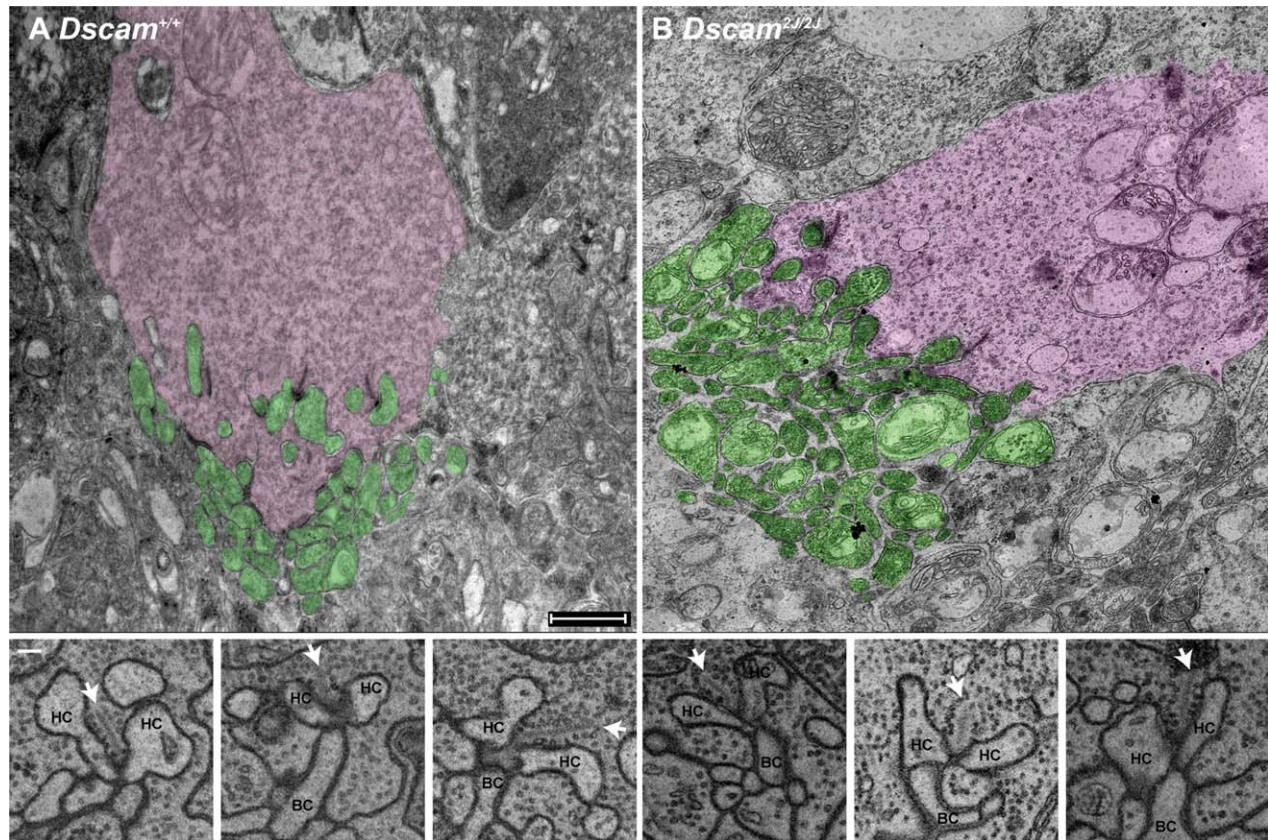
Figure 5. Cone synapse is present in the absence of *Dscam*. **A,B:** Electron microscopy of the adult (>P42) wild type and *Dscam*[2J/2J] cone pedicle and associated synapses, with the cone axon terminal labeled in pink and adjacent neurites labeled in green (*n* = 2 retinas each). Ribbons and associated structures appeared equivalent comparing wild-type and *Dscam*[2J/2J] retinas. Examples of high-resolution images of synaptic ribbons in which invaginating horizontal and bipolar cell processes can be observed adjacent to a ribbon, are shown underneath each genotype (arrow pointing at ribbon; HC, horizontal cell; BC, invaginating bipolar cell). Scale bar = 1 μm in upper left A (applies to upper A,B); 200 nm in lower left A (applies to lower A,B).

domain analysis is a measurement of the area around a given object, in this case the terminal of the cone axon, that is closer to that object than any other selected object, in this case other cone pedicles (Fig. 6C). The area around wild-type and *Dscam*[2J] pedicles was assayed, and the coefficients of variation, a measure of the variability of the area of Voronoi domains, of each genotype were compared by a Student's *t*-test. No significant difference in the variability of the domain size was detected (Fig. 6D). The density of cone terminals was also assayed in the wild type and *Dscam*[2J] retina. No significant difference in the density of pedicles was detected when comparing wild-type and *Dscam*[2J] retinas (Fig. 6E). This was repeated by assaying the central and peripheral retinas, which are more dense and sparse, respectively, in cones. A significant difference in the density of cones was detected when comparing central and peripheral regions of retina within or between genotypes, but no significant difference was detected when comparing like regions of retina

between genotypes (Fig. 6D,E). Therefore although *Dscam* may contribute to the organization of some cells that make synapses at the cone pedicle, we did not detect defects in the number or spacing of cone synapses.

We next focused on the two OFF bipolar cell types, type 3b and type 4, that appeared to have self-avoidance defects in the absence of *Dscam*. The organization of type 3b and type 4 dendrites was assayed by confocal microscopy in whole retinas. Clumping of type 4 bipolar cell dendrites (Fig. 7A–D) could be clearly observed in the *Dscam* mutant retina, whereas the axons and dendrites of other cell types appeared to be normal (Fig. 7E,F and data not shown).

Type 3b bipolar cells also appeared to have clumped dendrites in the *Dscam*[2J] retina (Fig. 8A,B). Bipolar cell bodies are not organized in mosaics in the mouse retina (Reese, 2011; Wässle and Riemann, 1978). The microanatomy of type 3b bipolar cells includes the projection of a dendrite stalk that forms a bulb-like
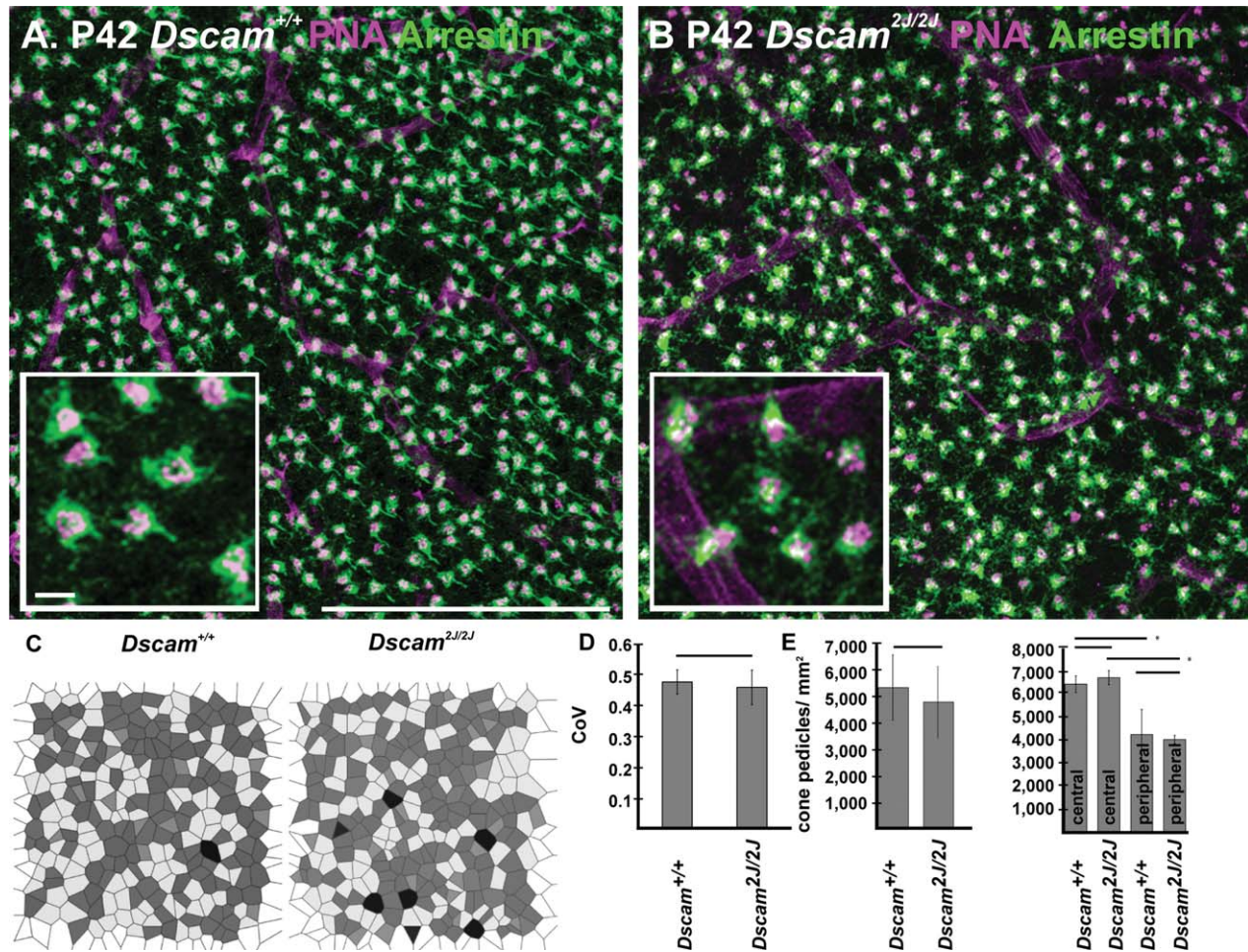
Figure 6. Spacing and number of cone pedicles is maintained in the absence of *Dscam*. **A,B:** Wild-type and *Dscam²ʲ/²ʲ* retinas were stained with antibodies to cone arrestin, to visualize cone pedicles, and PNA (higher magnification in inset). **C:** The spatial arrangement of cone pedicles was assayed by Voronoi domain analysis, which identifies the area around a pedicle that is closer to that pedicle than any other pedicle. **D:** No significant difference was detected in the coefficient of variance, the degree to which spatial domains vary in size, when comparing wild type and mutant. **E,F:** No significant difference in the number of pedicles was detected comparing wild-type and mutant retinas, although the density of pedicles was significantly higher in the central portion of the retina of both genotypes compared with the peripheral retina. Scale bar = 100 μm in A (applies to A,B); 5 μm in inset to A (applies to insets to A,B).

structure (heretofore referred to as the dendrite bulb) immediately before distal dendrites project out toward cone pedicles (Fig. 8A,B, insets) (Mataruga et al., 2007). The dendrite bulbs appeared to be spaced in the wild-type retina and clustered in the *Dscam²ʲ* retina, and provided a fixed point that could be used for spacing analysis, which typically uses the cell soma as a reference point. Spacing analysis was performed to test whether the dendrite bulbs of type 3b bipolar cells were clumped in the *Dscam²ʲ* retinas compared with wild type. Voronoi domain analysis was performed, using the most distal portion of the dendrite bulb (Fig. 8C). An apparent increase in dendrite bulbs with small or large Voronoi domains was noted, consistent with these structures being clumped in the *Dscam²ʲ* retina. A significant difference in the coefficient of variation

was detected when wild-type and *Dscam²ʲ* type 3b bipolar cell dendrite bulbs were compared (Fig. 8D).

Next, DRP was performed to determine whether there is a change in the spacing of *Dscam²ʲ* type 3b dendrite bulbs compared with wild type. DRP analysis is a measurement of the number of like structures within a given distance from a reference structure, measured for all such structures in a field (Rodieck, 1991). These data are then plotted out with the number of like events within a given distance from all of the objects collectively referred to as the reference soma (in this case the reference dendrite bulb). When objects are organized such that they avoid each other, an exclusion zone will exist wherein the number of counted objects falls below the average cell density. Because the size of such an exclusion zone would be expected to vary with
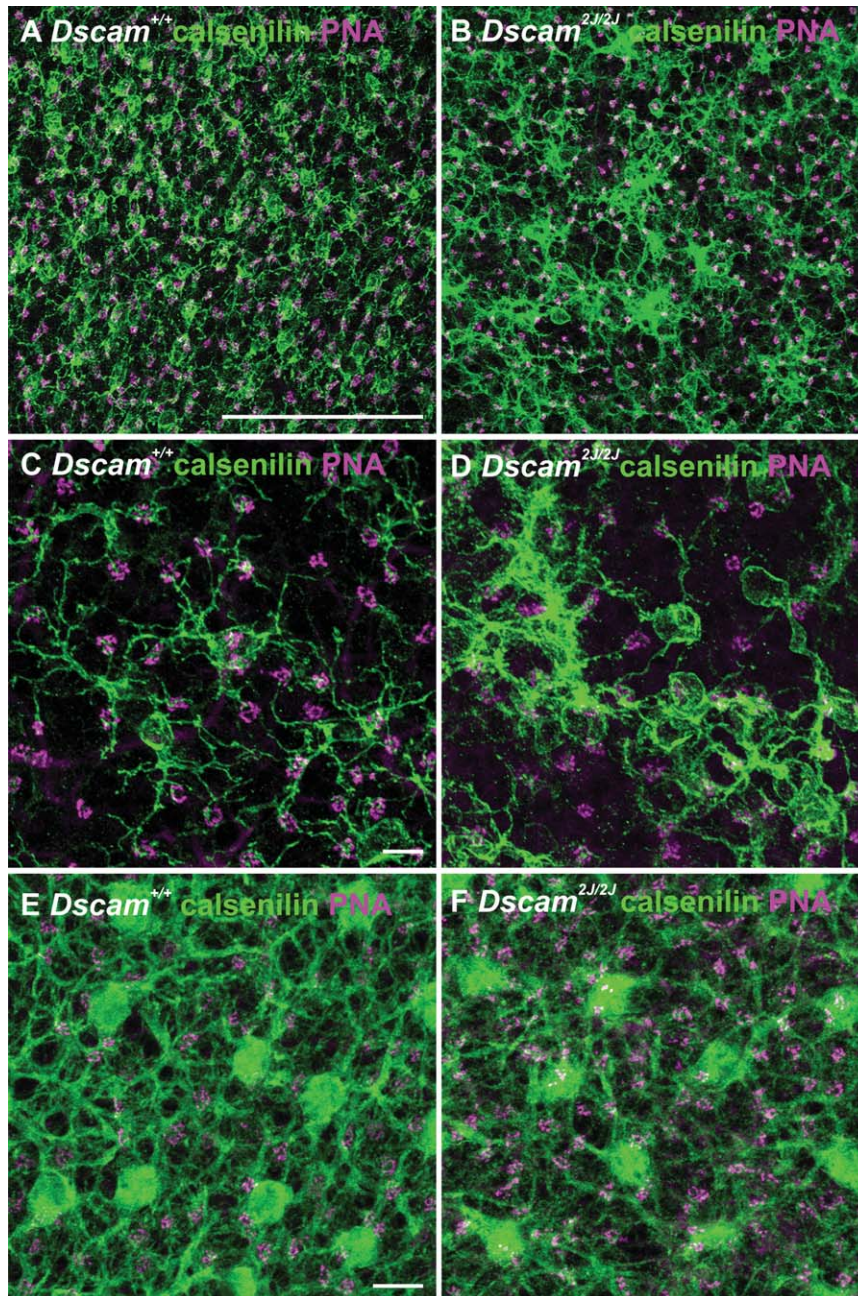
Figure 7. Clumping of calsenilin-positive bipolar cell dendrites in the *Dscam* mutant retina. **A–D:** Wild-type and *Dscam*$^{2J/2J}$ retinas were stained with antibodies to calsenilin, to label type 4 cone bipolar cells, and PNA (N > 4). Clumping of type 4 cone bipolar cell dendrites was observed in the *Dscam*$^{2J/2J}$ retina compared with wild type. **C,D:** At high magnification the projection of type 4 cone bipolar cell dendrites to cone pedicles can be observed in both the wild-type and *Dscam*$^{2J/2J}$ retinas. **E,F:** Wild-type and *Dscam*$^{2J/2J}$ retinas were stained with antibodies to calbindin, to label horizontal cells, and PNA (N > 4). A change in arborization of horizontal cell neurites was not observed in the *Dscam*$^{2J/2J}$ retina compared with wild type. Scale bar = 100 μm in A (applies to A,B); 10 μm in C (applies to C,D) and E (applies to E,F).

nificant increase in the density of type 3b bipolar cells was detected in the *Dscam*^{2J} retina compared with wild type (wild type average cell density 3,912 ± 214 vs. mutant average cell density 4,570 ± 221; $P = 0.02$). A significant difference ($P = 0.03$) was also detected when comparing the packing index of wild-type and *Dscam*^{2J} type 3b bipolar cell dendrite bulbs (Fig. 8E,F). The exclusion zone of wild-type 3b bipolar cells extended out to 10 μm from the reference soma, as indicated by a decrease in cell density compared with average cell density, whereas the exclusion zone reached average cell density in the *Dscam*^{2J} retina by 10 μm (Fig. 8E,F).

Finally, nearest neighbor analysis was performed. Nearest neighbor analysis is a measurement of the distance to the nearest neighbor, plotted for all objects in a field, and here is compared with a random distribution of a like number of objects in a like sized field. The nearest neighbor distances of both wild-type and *Dscam*^{2J} type 3b bipolar cell dendrite bulbs were significantly different than a random distribution, but the *Dscam*^{2J} type 3b bipolar cell dendrite bulbs were shifted toward random compared with wild type (P value comparing wild type and random = 0.00000009 vs. *Dscam*^{2J} vs. random = 0.007; Fig. 8G,H).

To understand the mechanism underlying the clumped type 3b and type 4 cone bipolar cell dendrites observed in the *Dscam*^{2J} retina, we tested whether this clumping was a secondary effect caused by changes in cell number and/or a disorganization of cells contributing to the inner plexiform layer. *Dscam* was targeted for deletion specifically in retinal ganglion cells using Brn3b-Cre to test the possibility that type 3b and type 4 cone bipolar cell dendrites are clumped secondarily to other cell types. Defects in type 3b and 4 cone bipolar cell dendrite arborization were observed in the *Dscam*^{FD} retina
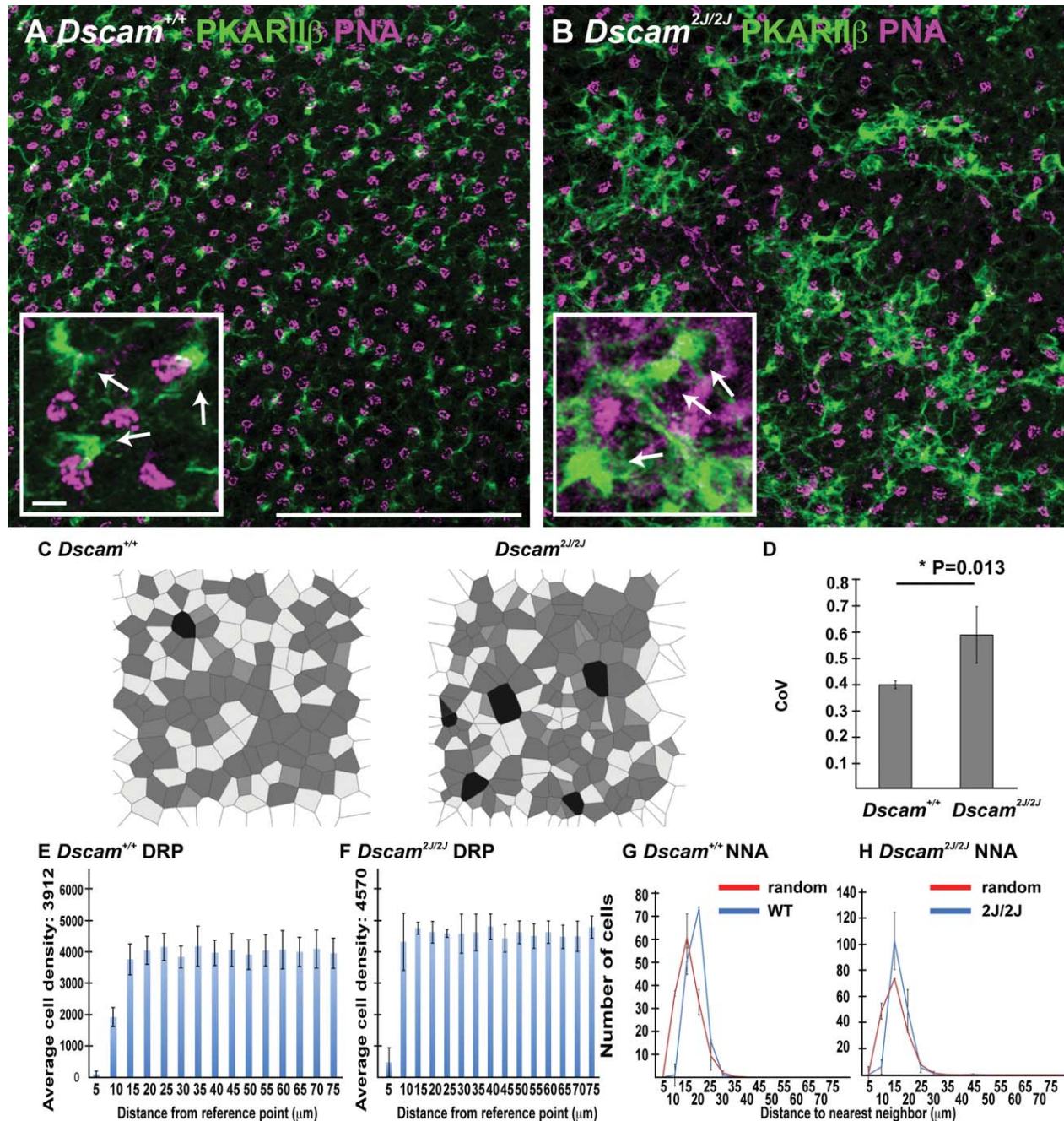
cell density, the size of the exclusion zone is translated into a value that is independent of cell density, the packing index. The packing index can then be used in statistical tests comparing different populations. A sig-

Figure 8. Disruption of type 3b cone bipolar cell dendrite arborization in the *Dscam*$^{2J/2J}$ retina. **A,B:** Whole adult (>P42) wild-type and *Dscam*$^{2J/2J}$ retinas were labeled with antibodies to PKARIIβ and PNA (N > 8 retinas). The dendrites of PKARIIβ-positive bipolar cells are clumped in the *Dscam*$^{2J/2J}$ retina compared with wild type. **C,D:** The location of the dendrite bulb, the portion of the dendrite stalk from which distal dendritic branches project, of each PKARIIβ bipolar cell was plotted and used to determine the Voronoi domains of these cells' dendrite bulbs in wild-type and *Dscam*$^{2J/2J}$ retinas (arrows point at sample dendrite bulbs; insets to A,B). **D:** Voronoi domain analysis revealed a statistically significant increase in the coefficient of variation (CoV) when comparing the Voronoi domains of wild-type and *Dscam*$^{2J/2J}$ type 3b bipolar cell dendrite bulbs. **E,F:** DRP analysis of PKARIIβ dendritic bulb spacing. A reduced exclusion zone was observed in close proximity to the reference soma in the *Dscam*$^{2J/2J}$ retina compared with wild-type controls (for example, at 10 μm from the reference soma), and a significant difference in the packing factor was detected when comparing genotypes (*P* = 0.03). **G,H:** Nearest neighbor analysis of type 3b bipolar cells in wild-type and *Dscam*$^{2J/2J}$ retinas. Distribution of dendrite bulbs in both genotypes was significantly different from random simulations, and a decrease in the average distance to the nearest neighbor was detected in the *Dscam*$^{2J/2J}$ retina compared with wild type. Scale bar = 100 μm in A (applies to A,B); 5 μm in inset to A (applies to insets to A,B).
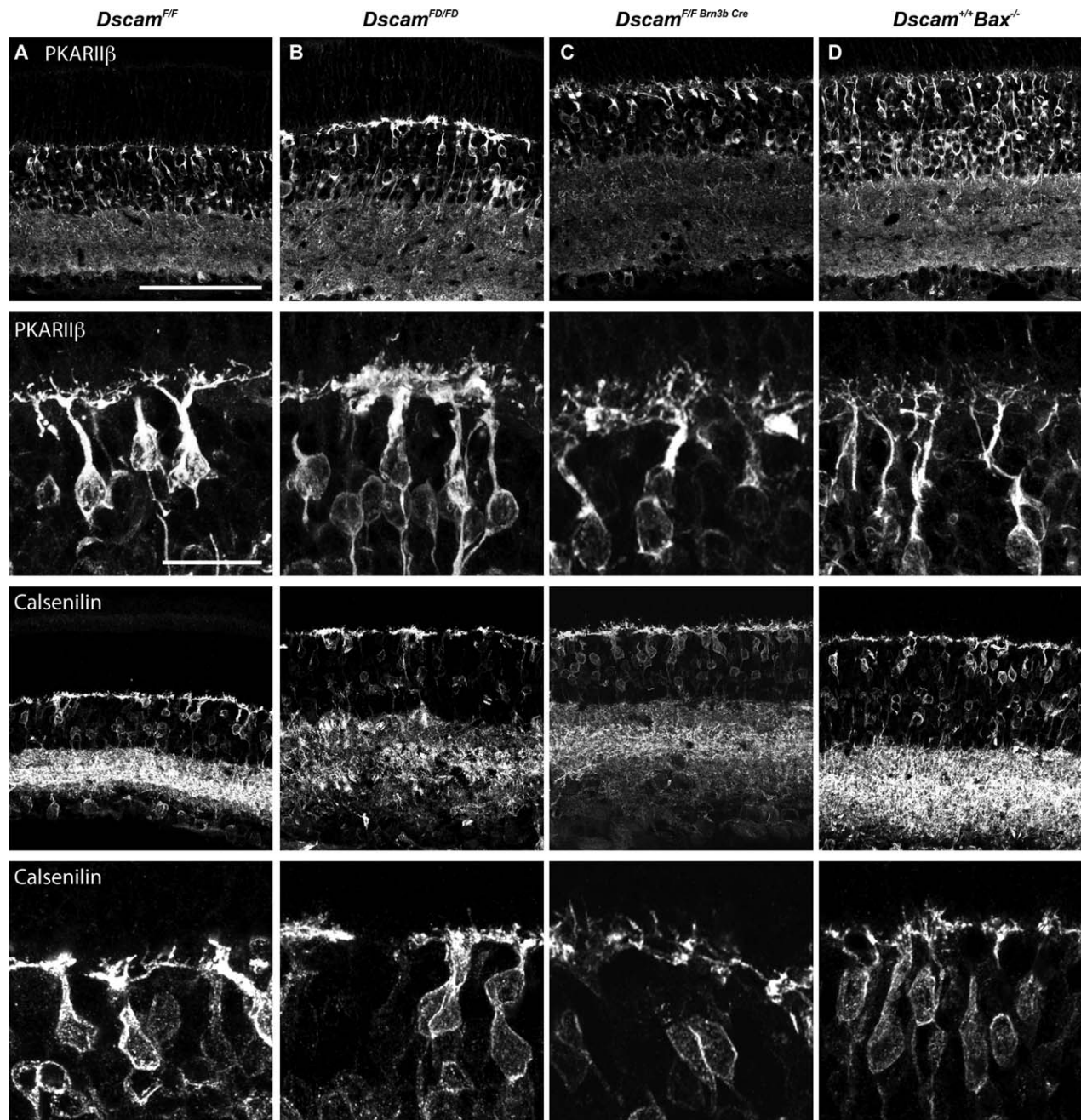
Figure 9. Clumping of type 3b and type 4 bipolar cell dendrites is not observed when *Dscam* was specifically targeted in RGCs or in the Bax null retina. **A–D:** Sections of retina from adult (P42 or older) unrecombined conditional allele of *Dscam* (*Dscam^F/F*; A) or the conditional allele of *Dscam* targeted for deletion in the germline (*Dscam^FD/FD*; B) or the conditional allele of *Dscam* targeted in retinal ganglion cells (*Dscam^F/F Brn3b-Cre*; C) or Bax null (*Dscam^+/+ Bax^−/−*; D) mice were stained with antibodies to PKARIIβ or calsenilin, to label type 3b or type 4 cone bipolar cells, respectively (*n* = 3 for each genotype). **A:** The dendrites of type 3b and type 4 cone bipolar cells were not clumped in the *Dscam^F/F* retina. **B:** The dendrites of type 3b and type 4 cone bipolar cells were clumped in the *Dscam^FD/FD* retina. **C,D:** The dendrites of type 3b and type 4 cone bipolar cells were not clumped in the *Dscam^F/F Brn36 Cre* or *Bax−/−* retinas. Scale bar = 100 μm in A, row 1 (applies to rows 1 and 3); 20 μm in A, row 2 (applies to rows 2 and 4).

compared with the *Dscam^F* retina, indicating that deletion of the *Dscam* transmembrane domain, targeted in the conditional allele, is sufficient to cause this dendrite clumping and that arborization resembles wild type in the floxed *Dscam^F* allele in the absence of Cre recombinase (Fig. 9A,B). Type 3b and type 4 cone bipolar cell dendrites do not clump if *Dscam* is targeted for deletion in retinal ganglion cells, despite the widespread
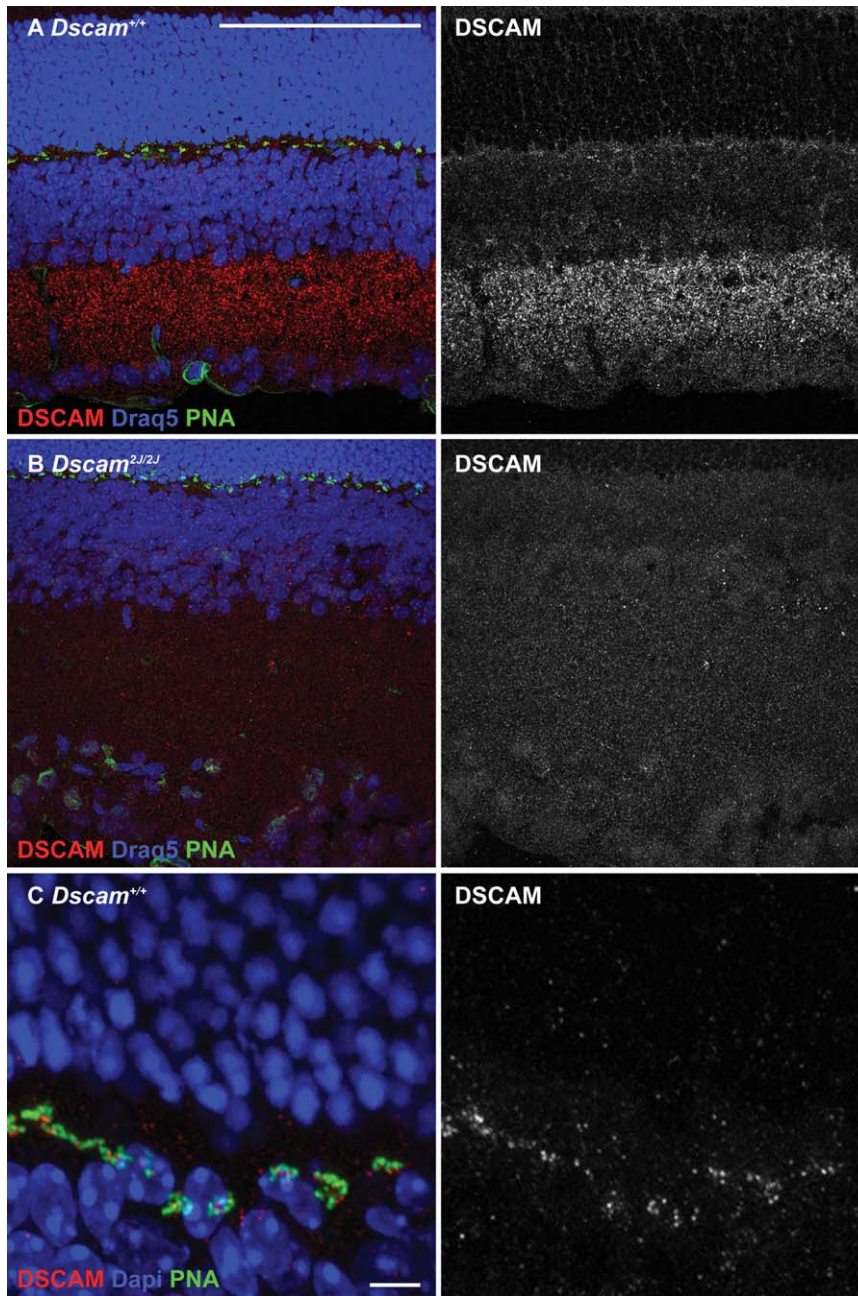
Figure 10. DSCAM localization in the mouse retina. **A–C:** Sections of wild-type and *Dscam*[2J/2J] retinas were stained with antibodies to DSCAM (N > 8 for both genotypes). **A:** DSCAM immunoreactivity was observed throughout the inner plexiform layer of the wild-type adult retina. **B:** This immunoreactivity was not observed in the *Dscam*[2J/2J] retina. **C:** DSCAM immunoreactivity was observed in close proximity to the cone synapse in the outer plexiform layer. Scale bar = 100 μm in A (applies to A,B); 10 μm in C.

clumping of bipolar cell dendrites. To do so, we assayed the organization of dendrites in the *Bax* null retina, in which normal developmental cell death is blocked and a large increase in cell number is observed (Knudson et al., 1995; Mosinger Ogilvie et al., 1998). Although deletion of Bax is sufficient to cause clumping of cell soma and dendrites of some retinal cell types, similar to what is observed in the *Dscam* heterozygous retina, defects in type 3b and type 4 cone bipolar cell dendrites were not observed in the *Bax* null retina (Fig. 9D) (Chen et al., 2013; Keeley et al., 2012).

The localization and cell type–specific expression of *Dscam* was assayed to understand why some populations of cone bipolar cells had clumped dendrites in the absence of DSCAM. Previous studies of DSCAM localization found limited staining in the retina and did not detect protein in many cell types in which *Dscam* mRNA was detected, likely as a result of antigen inactivation during the prolonged fixation used in this study (Fuerst et al., 2008). We therefore screened DSCAM antibodies using transfected cells and wild-type and *Dscam* null retinas and optimized staining procedures for DSCAM. Multiple antibodies were identified that stained DSCAM with a high level of specificity in cell culture (Fig. 1C). One of these, a monoclonal antibody, was identified that had a high degree of specificity in immunohistochemical staining of the retina with low background. DSCAM protein was localized throughout the synaptic inner plexiform layer of the adult mouse

disorganization of retinal ganglion cells and some secondary disorganization of amacrine cells when the floxed allele of *Dscam* is targeted with Brn3b-Cre (Fig. 9A–C) (Fuerst et al., 2012).

A large increase in cell number is also observed in the *Dscam* mutant retina, and we sought to test whether increased cell number was sufficient to cause

retina and in the synaptic outer plexiform layer (Fig. 10A). Specificity was verified by the lack of staining in *Dscam*[2J] mice, which have previously been shown to lack DSCAM by western blot analysis (Fig. 10B) (Schramm et al., 2012). Sections of mouse retina were labeled with PNA, which labels the invaginating tips of ON bipolar cells, and DSCAM. DSCAM immunoreactivity
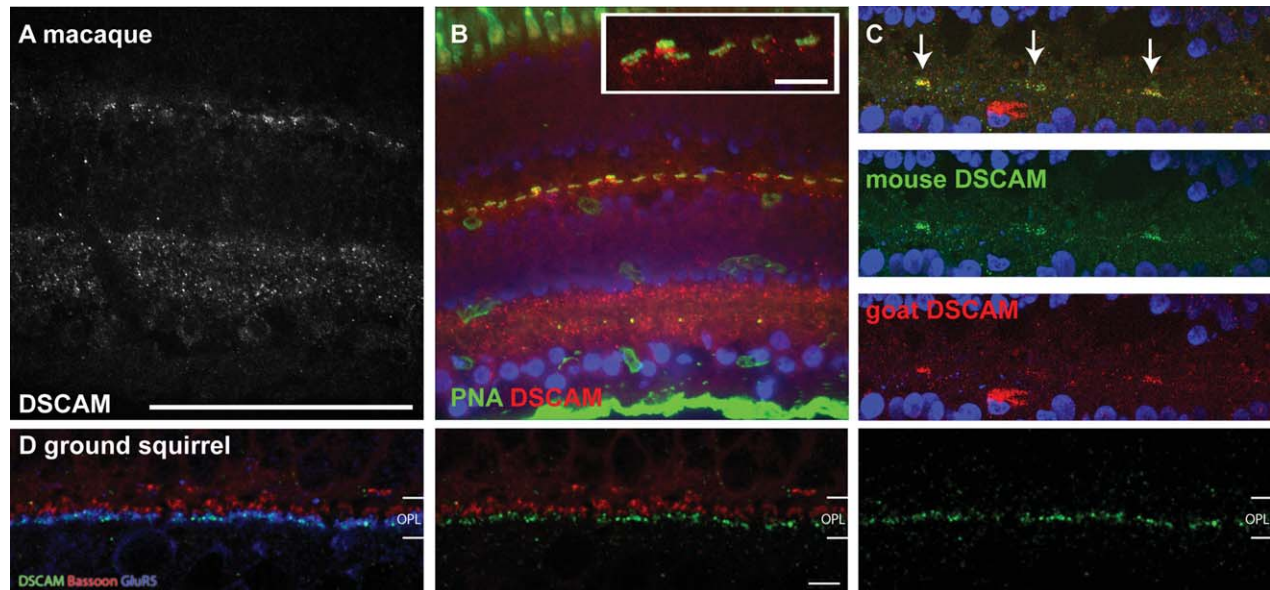
Figure 11. DSCAM localization in macaque and ground squirrel retina. Sections of macaque and ground squirrel were stained with antibodies to DSCAM and PNA (macaque) or DSCAM, GluR5, and Bassoon (ground squirrel) ($n = 2$ retinas). **A:** DSCAM immunoreactivity was observed in the macaque inner and outer plexiform layers. In the inner plexiform layer DSCAM was concentrated in the lamina proximal to the two cellular layers and was less concentrated in the central inner plexiform layer. **B:** DSCAM immunoreactivity was observed proximal to the inner nuclear layer with respect to PNA staining in the macaque retina. **C:** Specificity of DSCAM immunoreactivity in the macaque outer plexiform layer was confirmed by using DSCAM antibodies generated in two different species. **D:** DSCAM immunoreactivity in the ground squirrel outer plexiform layer was observed running along GluR5, a receptor expressed by OFF bipolar cells, but not running alongside Bassoon, a presynaptic marker. Scale bar = 100 μm in A (applies to A–C); 5 μm in inset to B; 5 μm in D.

was concentrated adjacent to PNA labeling (Fig. 10C). The localization of DSCAM in two cone dominant species, macaque and ground squirrel, was also assayed. DSCAM staining was observed on the inner nuclear layer facing side of PNA staining in the macaque retina (Fig. 11A–C). A similar pattern of postsynaptic localization was observed in ground squirrel retina (Fig. 11D).

Next DSCAM was localized during development of the outer plexiform layer, identified with PSD95 staining. DSCAM protein was observed to roughly overlap with PSD95 staining until approximately postnatal day 12, after which DSCAM was observed proximal to the inner nuclear layer with respect to PNA and PSD95 staining (Fig. 12). Some DSCAM staining was also observed in outer plexiform layer proximal cells in the inner nuclear layer, especially between postnatal days 8 and 12 (Fig. 12).

The expression of *Dscam* in bipolar and horizontal cells was assayed to determine whether cell type–specific expression could explain the clumping of some OFF bipolar cells in the absence of DSCAM. We took advantage of the retention of DSCAM protein produced by the *Dscam*^FD allele, which lacks a transmembrane domain. DSCAM accumulates around the soma in the *Dscam*^FD retina (Fig. 13A,B). Staining with DSCAM and one or more cell type–specific antigens was performed

to identify cell types that express *Dscam*, for example, some calbindin-positive cells express *Dscam*, but not the cholinergic subset (Fig. 13C). Next, cell types in which *Dscam* expression was previously assayed by in situ hybridization were assayed to verify this technique (Fuerst et al., 2008, 2009). Protein was observed in cell types previously shown to express *Dscam* (bNOS-positive amacrine cells and retinal ganglion cells) but was not observed in those in which *Dscam* transcript was not previously observed (cholinergic and AII amacrine cells) (Fig. 14A–D).

Next the presence of DSCAM was assayed in bipolar and horizontal cells. DSCAM protein was observed in HCN4-, calsenilin-, PKARIIβ-, and some Syt-2 positive bipolar cells, but was not observed in PKCα-, NK3R-, or recoverin-positive bipolar cells or in horizontal cells (Table 2 and Fig. 14E–P). The presence of DSCAM in type 3b and type 4 bipolar cells is consistent with the dendrite arborization defects observed in these cell types. The lack of a dendrite arborization phenotype in the type 3a and Syt2-immunopositive phenotype could be due to an absence of DSCAM protein at the dendrites (i.e., if it is localized to the bipolar cell axon of these cells). The localization of DSCAM to dendrite tips was assayed in type 3a, type 3b, type 4, and
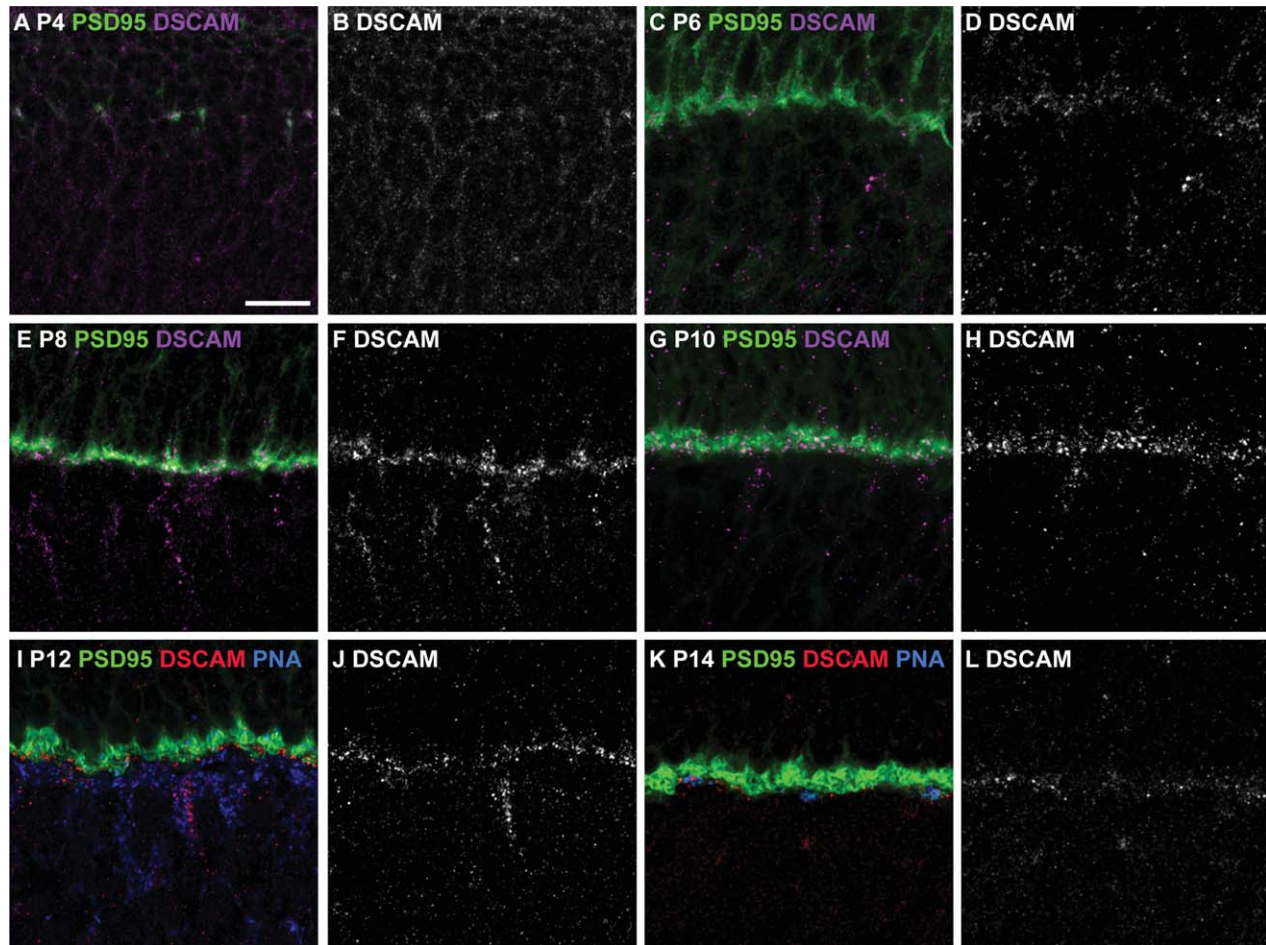
Figure 12. Developmental localization of DSCAM in the outer plexiform layer. **A–H:** Sections of mouse retina stained with antibodies to DSCAM and PSD95 (*n* = 4 retinas at each age). **A,B:** At P4, DSCAM and PSD95 immunoreactivity overlap. **C,D:** At P6, DSCAM immunoreactivity has taken on a punctate pattern nested within PSD95 immunoreactivity. **E,F:** At P8, DSCAM immunoreactivity is observed as puncta within areas immunoreactive for PSD95 and within the soma of cells in the developing inner nuclear layer. **G,H:** At P10, DSCAM immunoreactivity is observed in puncta overlapping with areas stained by PSD95 and in cell soma in the developing inner nuclear layer. Puncta of DSCAM and PSD95 immunoreactivity that do not overlap with each other become more apparent. **I,J:** By P12, DSCAM immunoreactivity begins to become confined to the inner face of PSD95 immunoreactivity. **K,L:** By P14, DSCAM immunoreactivity is closely associated with PNA staining and is largely distinct from PSD95 immunoreactivity. Scale bar = 10 μm in A (applies to A–L).

Syt2-immunopositive bipolar cells. The number of puncta localizing at the tips of each of these bipolar cell types was counted compared with the total number of puncta. Type 3b and type 4 bipolar cells were found to have more DSCAM localized to their tips (30 and 54% of puncta, respectively), compared with type 3a and Syt2-positive cells (11 and 9%, respectively) (Fig. 15). The number of puncta overlapping with type 3a and type 4 dendrites was reduced when the channel containing the bipolar cell dendrites was flipped along the horizontal axis (type 3b: 30–18% and type 4: 54–16%). The number of puncta overlapping with the dendrites of type 3a and Syt2-immunopositive cells remained similar when the channel containing the dendrite staining was flipped along the horizontal axis (type

3a: 11–14% and Syt2-immunopositive cells 9–14%), suggesting that the amount of DSCAM protein observed at the dendritic tips of these cells may reflect coincident staining.

DISCUSSION

Understanding how individual cells are integrated into the functional circuitry of the nervous system is a central goal of neuroscience. In recent years, loss and gain of function analysis has begun to identify genes required for the integration of cells into neural circuits, but much work remains in order to understand how the proteins these genes encode mediate their functions.

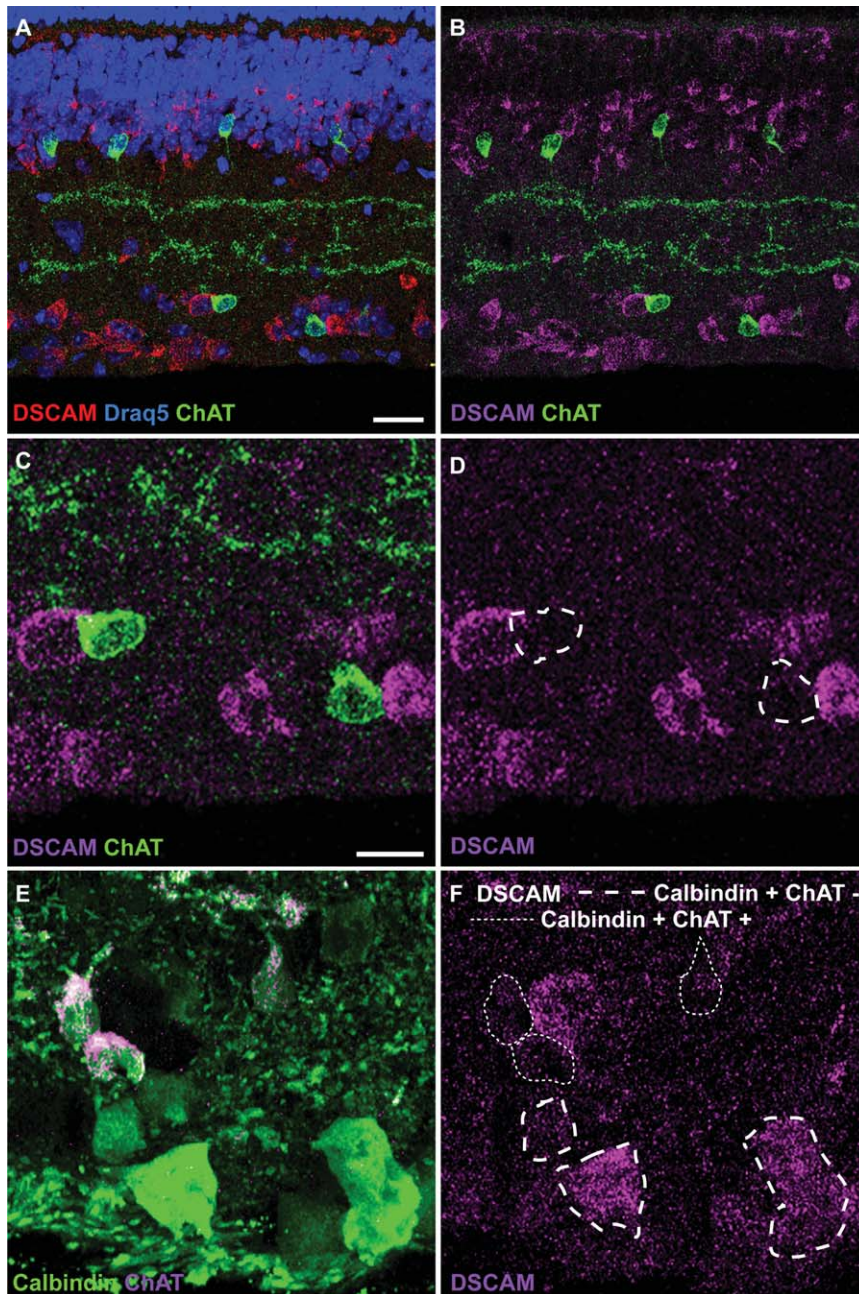DSCAMs were first functionally studied in *Drosophila*, in which the incredible splice diversity of Dscam1

Figure 13. Use of a cytoplasmic isoform of DSCAM to identify cell types that produce the protein. **A–D:** Sections of *Dscam*[FD/FD] retina were stained with antibodies to DSCAM and ChAT and stained with Draq5, to label nuclei. The DSCAM protein produced by the *Dscam*[FD/FD] allele lacks a transmembrane domain and accumulates in the cell cytosol. **A,B:** DSCAM immunoreactivity is observed in most cells in the retinal ganglion cell layer, in many cells in the RGL proximal portion of the inner nuclear layer, and in some cells in the outer portion of the inner nuclear layer. DSCAM immunoreactivity was not observed in ChAT-immunoreactive cells. **C,D:** Higher magnification of section from A and B. **E,F:** Sections of *Dscam*[FD/FD] retina were stained with antibodies to DSCAM, calbindin, and ChAT. **E:** ChAT is expressed by some but not all calbindin-positive cells. DSCAM immunoreactivity was not observed in ChAT-positive cells but was observed in a subset of calbindin-positive ChAT-negative cells. Scale bar = 10 μm in A (applies to A,B); 5 μm in C (applies to C–F).

mediates specificity of neural development (Schmucker et al., 2000). Other *Drosophila* Dscam proteins that do not undergo extensive alternative splicing also play important neurodevelopmental roles. For example, *Drosophila* Dscam2 mediates synaptic specificity in conjunction with Dscam1 at the fly tetrad synapse by providing a repulsive cue (Millard et al., 2010). Indeed, it will be interesting to test whether mouse DSCAM mediates innervation of the multi-contact cone synapse so as to limit the number of connections made at each pedicle, analogous to the function of Dscams in organization of the tetrad synapse in *Drosophila*. Dscams in the mouse retina are required for a number of different developmental events, including regulation of cell number, normal spacing of soma, arborization of dendrites, and refinement of retinal ganglion cell axons in the lateral geniculate nucleus (Blank et al., 2011; Fuerst et al., 2008, 2009). Although Dscams appear to mediate repulsion in both fly and mouse, the neurites of many cell types in the mouse retina that clump in the absence of *Dscam* do not actively avoid each other, unlike *Drosophila* type IV DA neurons, (Keeley and Reese, 2010). This suggests that the adhesion observed in the *Dscam* mutant retina is not because DSCAM directly mediates repulsion and has been interpreted to suggest that DSCAM prevents adhesion of cell type–specific identifiers (Garrett et al., 2012). This is consistent with the observation that many spatially overlapping cell types require *Dscam* to prevent adhesion, but when they do adhere they do so according to cell type. Indeed, a simple explanation to explain why some cell types that express *Dscam* do not adhere in its absence is that they may not

produce a protein that causes such adhesion in the absence of *Dscam*.

In further considering the function of *Dscam* in development of the cone synapses, one might first consider the various requirements necessary for organization of such a structure. Each cone axon terminal is contacted by multiple bipolar and horizontal cells, which in turn send dendrites to distinct cone terminals. Therefore cells must not only make the correct synaptic contacts but also must avoid making multiple contacts at the same pedicle, so as to sample multiple pedicles. At a minimum this would require cells to have a mechanism to recognize their synaptic targets (heteroneuronal recognition between cell types), like cells (heteroneuronal recognition within cell types) and processes originating from the same cell (isoneuronal recognition).
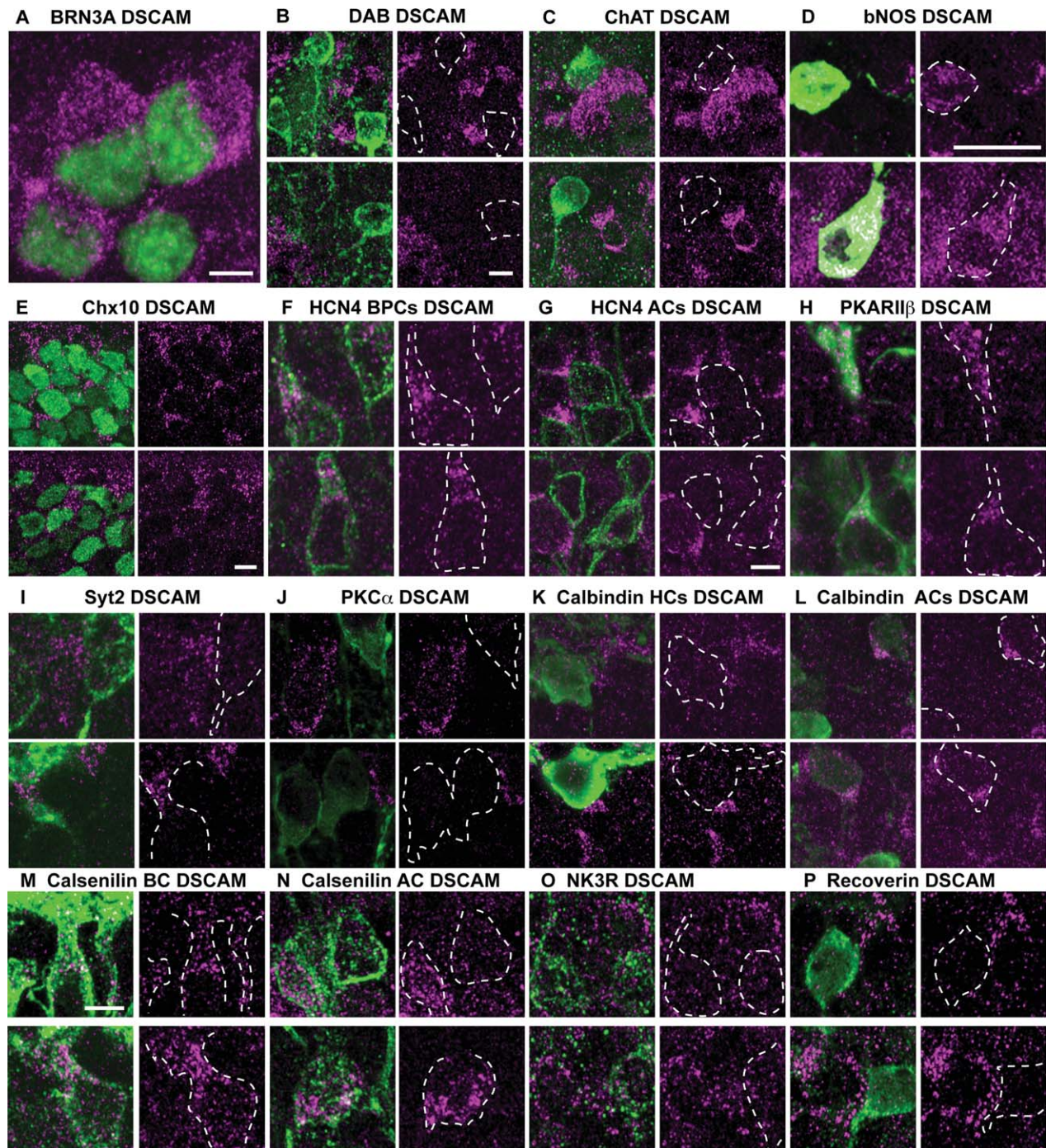

Figure 14.

Mechanisms to mediate this include but are not limited to synaptic activity, glial stimulation, and neural recognition through cell adhesion molecules. Although glia are important facilitators of neural development and connectivity in other parts of the nervous system, their role in development of the cone synapse appears to be limited in that normal development occurs in their absence (Williams et al., 2010). Likewise, whereas activity is required for maintenance of photoreceptor synapses, they appear to develop normally in its absence (Claes et al., 2004). Based on these and other studies, better candidates for mediating organization of the cone synapse appear to be cell adhesion molecules.

TABLE 2.
Dscam-Expressing Cell Types in the Inner Nuclear Layer

Cell type	Marker	*Dscam* expression
Type 1 and 2 bipolar cells	NK3R	Negative
Type 2 bipolar cells	Recoverin	Negative
Type 3a bipolar cells	HCN4	Positive
Type 3b bipolar cells	PKARIIβ	Positive
Type 4 bipolar cells	Calsenilin	Positive
Type 2 or type 6 bipolar cell	Syt2	Mixed
Rod bipolar cells	PKCα	Negative
Horizontal cells	Calbindin	Negative
HCN4+ amacrine cells	HCN4	Negative
Calsenilin-positive amacrine cells	Calsenilin	Mixed
Calbindin/ChAT-positive amacrine cells	Calbindin/ChAT	Mixed

Current research in understanding the role of adhesion molecules in developmental organization of neurons is focused on identifying factors such as Dscams, sidekicks, semaphorins and plexins, and the γ-protocadherins that provide the adhesive and repulsive cues required to properly wire the nervous system. Evidence for the role of cell adhesion molecules in organization of the cone synapse can be inferred by defects in development that occur in their absence. For example, horizontal cells utilize mouse epidermal growth factor (mEGF) proteins, semaphorins, and plexins to mediate self-avoidance (Kay et al., 2012; Matsuoka et al., 2011) and netrin-G ligand 2 (NGL-2) to properly innervate the rod spherule (Soto et al., 2013). The identification of factors regulating organization of the dendrites and axons of other cells composing the photoreceptor synapses is not currently as advanced, although homotypic regulation clearly regulates organization of the dendrite field of type 7 cone bipolar cells (Lee et al., 2011). Previously we have shown that *Dscaml1* is required for arborization of rod bipolar cell dendrites, but a role for DSCAM in the organization of outer plexiform layer cells had not been assayed.

In this study we identify DSCAM as a regulator of cell type–specific avoidance in two populations of OFF bipolar cells, analogous to the role of MEGF proteins in horizontal cells. The role of DSCAM in heteroneuronal interactions between cell types at the cone pedicle remains an open question, as does the resulting

Figure 14. *Dscam* is expressed by some OFF bipolar cell populations. **A:** Section of *Dscam*[FD/FD] retina stained with antibodies to DSCAM and Brn3A (n = 2). DSCAM immunoreactivity was observed in the soma of Brn3A-positive cells in the retinal ganglion cell layer. **B:** Section of *Dscam*[FD/FD] retina stained with antibodies to DSCAM and disabled (Dab) to stain AII amacrine cells (n = 2). AII amacrine cells did not contain DSCAM in their soma. **C:** Section of *Dscam*[FD/FD] retina stained with antibodies to DSCAM and ChAT, to label cholinergic amacrine cells (n = 2). Cholinergic amacrine cell soma in the inner nuclear layer (top) or retinal ganglion layer (bottom) did not contain DSCAM protein. **D:** Section of *Dscam*[FD/FD] retina stained with antibodies to DSCAM and bNOS (n = 2). bNOS-positive amacrine cells in both the inner nuclear layer (top) and retinal ganglion cell layer (bottom) contained DSCAM protein in their soma. **E:** Section of *Dscam*[FD/FD] retina stained with antibodies to DSCAM and Chx10, to label bipolar cells (n = 4). DSCAM immunoreactivity was observed in the soma surrounding some Chx10 positive cells. **F,G:** Section of *Dscam*[FD/FD] retina stained with antibodies to HCN4 to label a subset of amacrine cells (G) and type 3a cone bipolar cells (F) (n = 2 retinas). **F:** HCN4-positive bipolar cells, distinguished from amacrine cells by projection of dendrites to the outer plexiform layer and location, contained DSCAM protein in their soma. **G:** HCN4-positive amacrine cells, identified by their location proximal to the inner plexiform layer, did not contain DSCAM protein. **H:** Sections of *Dscam*[FD/FD] retina were stained with antibodies to DSCAM and PKARIIβ to label type 3b bipolar cells. DSCAM immunoreactivity was observed in PKARIIβ-positive cells. **I:** Sections of *Dscam*[FD/FD] retina were stained with antibodies to DSCAM and Syt2, to label type 2 and type 6 bipolar cells (n = 2 retinas). Some Syt2-immunopositive cells contained DSCAM immunoreactivity, and others did not. **J:** Sections of *Dscam*[FD/FD] retina were stained with antibodies to DSCAM and PKCα, to label rod bipolar cells. PKCα-immunopositive cells did not contain DSCAM. **K,L:** Sections of *Dscam*[FD/FD] retina were stained with antibodies to calbindin to label horizontal cells (K) and a subset of amacrine cells (L) (n = 4 retinas). **K:** Horizontal cells, identified by their location close to the outer plexiform layer, did not contain DSCAM. **L:** Dimly staining calbindin-positive (ChAT-negative) amacrine cells located within the inner nuclear layer contained DSCAM protein. **M,N:** Sections of *Dscam*[FD/FD] retina were stained with antibodies to calsenilin to label type 4 cone bipolar cells (M) and a subset of amacrine cells (N) (n = 4 retinas). **M:** DSCAM immunoreactivity was observed in calsenilin-positive bipolar cells. **N:** DSCAM protein was observed in some calsenilin-positive amacrine cells, identified by their location in the inner nuclear layer. **O:** Sections of *Dscam*[FD/FD] retina were stained with antibodies to DSCAM and NK3R, to label type 1 and 2 cone bipolar cells. NK3R-immunopositive cells did not contain DSCAM. **P:** Sections of *Dscam*[FD/FD] retina were stained with antibodies to DSCAM and recoverin, to label type 2 cone bipolar cells. Recoverin-immunopositive cells did not contain DSCAM. Scale bar = 5 μm in A (applies to A,F,H,I), B (applies to B,C), D, E, G (applies to G,J,L), and M (applies to M–P).
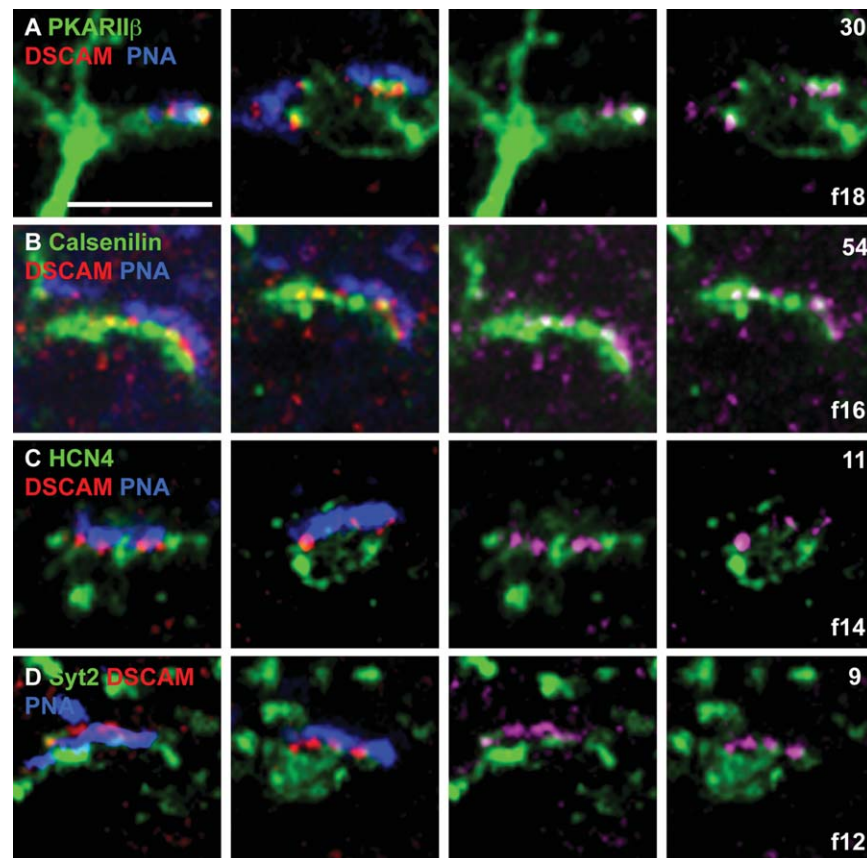
Figure 15. DSCAM localization on bipolar cell dendrites. B>A–D: Sections of wild-type adult (>P42) retina stained with antibodies to DSCAM and PKARIIβ, calsenilin, HCN4, or Syt2 and PNA ($n = 4$ retinas). DSCAM immunoreactivity was observed at the ends of some cone bipolar cell dendrite tips that terminated at the cone pedicle. The percent of DSCAM puncta that were observed within the dendrites of the respective bipolar cell types was counted for 20 pedicles and is reported in the upper corner of the left most panel. The result of this count when the channel containing bipolar cell staining was flipped along the horizontal axis is reported in the lower left hand corner. Scale bar = 5 μm in A (applies to A–D).

physiology at disorganized cone synapses. Recently the role of Dscam1 overexpression in the *Drosophila* nervous system has been demonstrated and linked to fragile-X syndrome (Cvetkovska et al., 2013; Kim et al., 2013). Preliminary results indicate that DSCAM over and or ectopic expression in the cells contributing to the mouse cone synapse disrupt this structure, and that this line of approach together with targeted loss of function will be an extremely powerful tool in understanding the function of DSCAM in heteroneuronal interactions between like and non-like cell types, its role in human diseases, and the developmental organization of the cone synapse and other synapses.

CONFLICT OF INTEREST STATEMENT

The authors have no conflict of interest with respect to this work.

ROLE OF AUTHORS

All authors had full access to all the data in the study and take responsibility for the integrity of the data and the accuracy of the data analysis. Study concept and design: PGF. Acquisition of data: GBA, SSL, HF, WL, and PGF. Analysis and interpretation of data: PGF and WL. Drafting of the manuscript: PGF. Critical revision of the manuscript for important intellectual content: PGF. Statistical analysis: PGF. Obtained funding: PGF. Administrative, technical, and material support: PGF and WL. Study supervision: PGF.

LITERATURE CITED

Blank M, Fuerst PG, Stevens B, Nouri N, Kirkby L, Warrier D, Barres BA, Feller MB, Huberman AD, Burgess RW, Garner CC. 2011. The Down syndrome critical region regulates retinogeniculate refinement. J Neurosci 31: 5764–5776.

Boycott BB, Hopkins JM. 1991. Cone bipolar cells and cone synapses in the primate retina. Vis Neurosci 7:49–60.

Burke MC, Letts PA, Krajewski SJ, Rance NE. 2006. Coexpression of dynorphin and neurokinin B immunoreactivity in the rat hypothalamus: morphologic evidence of interrelated function within the arcuate nucleus. J Comp Neurol 498:712–726.

Burmeister M, Novak J, Liang MY, Basu S, Ploder L, Hawes NL, Vidgen D, Hoover F, Goldman D, Kalnins VI, Roderick TH, Taylor BA, Hankin MH, McInnes RR. 1996. Ocular retardation mouse caused by Chx10 homeobox null allele: impaired retinal progenitor proliferation and bipolar cell differentiation. Nat Genet 12:376–384.

Chen S, Li W. 2012. A color-coding amacrine cell may provide a blue-off signal in a mammalian retina. Nat Neurosci 15:954–956.

Chen SK, Chew KS, McNeill DS, Keeley PW, Ecker JL, Mao BQ, Pahlberg J, Kim B, Lee SC, Fox MA, Guido W, Wong KY, Sampath AP, Reese BE, Kuruvilla R, Hattar S. 2013. Apoptosis regulates ipRGC spacing necessary for rods and cones to drive circadian photoentrainment. Neuron 77:503–515.

Claes E, Seeliger M, Michalakis S, Biel M, Humphries P, Haverkamp S. 2004. Morphological characterization of the retina of the CNGA3(-/-)Rho(-/-) mutant mouse lacking functional cones and rods. Invest Ophthalmol Vis Sci 45:2039–2048.

Cvetkovska V, Hibbert AD, Emran F, Chen BE. 2013. Overexpression of Down syndrome cell adhesion molecule impairs precise synaptic targeting. Nat Neurosci 16:677–682.

Dick O, tom Dieck S, Altrock WD, Ammermuller J, Weiler R, Garner CC, Gundelfinger ED, Brandstätter JH. 2003. The presynaptic active zone protein bassoon is essential for photoreceptor ribbon synapse formation in the retina. Neuron 37:775–786.

Fox MA, Sanes JR. 2007. Synaptotagmin I and II are present in distinct subsets of central synapses. J Comp Neurol 503:280–296.

Fuerst PG, Koizumi A, Masland RH, Burgess RW. 2008. Neurite arborization and mosaic spacing in the mouse retina require DSCAM. Nature 451:470–474.

Fuerst PG, Bruce F, Tian M, Wei W, Elstrott J, Feller MB, Erskine L, Singer JH, Burgess RW. 2009. DSCAM and DSCAML1 function in self-avoidance in multiple cell types in the developing mouse retina. Neuron 64:484–497.

Fuerst PG, Harris BS, Johnson KR, Burgess RW. 2010. A novel null allele of mouse DSCAM survives to adulthood on an inbred C3H background with reduced phenotypic variability. Genesis 48:578–584.

Fuerst PG, Bruce F, Rounds RP, Erskine L, Burgess RW. 2012. Cell autonomy of DSCAM function in retinal development. Dev Biol 361:326–337.

Garrett AM, Tadenev AL, Burgess RW. 2012. DSCAMs: restoring balance to developmental forces. Front Mol Neurosci 5:86.

Hack I, Peichl L, Brandstätter JH. 1999. An alternative pathway for rod signals in the rodent retina: rod photoreceptors, cone bipolar cells, and the localization of glutamate receptors. Proc Natl Acad Sci U S A 96:14130–14135.

Haverkamp S, Wässle H. 2000. Immunocytochemical analysis of the mouse retina. J Comp Neurol 424:1–23.

Haverkamp S, Grünert U, Wässle H. 2000. The cone pedicle, a complex synapse in the retina. Neuron 27:85–95.

Haverkamp S, Ghosh KK, Hirano AA, Wässle H. 2003. Immunocytochemical description of five bipolar cell types of the mouse retina. J Comp Neurol 455:463–476.

Haverkamp S, Specht D, Majumdar S, Zaidi NF, Brandstätter JH, Wasco W, Wässle H, Tom Dieck S. 2008. Type 4 OFF cone bipolar cells of the mouse retina express calsenilin and contact cones as well as rods. J Comp Neurol 507:1087–1101.

Hopkins JM, Boycott BB. 1992. Synaptic contacts of a two-cone flat bipolar cell in a primate retina. Vis Neurosci 8: 379–384.

Kay JN, Chu MW, Sanes JR. 2012. MEGF10 and MEGF11 mediate homotypic interactions required for mosaic spacing of retinal neurons. Nature 483:465–469.

Keeley PW, Reese BE. 2010. Morphology of dopaminergic amacrine cells in the mouse retina: independence from homotypic interactions. J Comp Neurol 518:1220–1231.

Keeley PW, Sliff BJ, Lee SC, Fuerst PG, Burgess RW, Eglen SJ, Reese BE. 2012. Neuronal clustering and fasciculation phenotype in Dscam- and Bax-deficient mouse retinas. J Comp Neurol 520:1349–1364.

Khiripet N, Khantuwan W, Jungck JR. 2012. Ka-me: a Voronoi image analyzer. Bioinformatics 28:1802–1804.

Kim JH, Wang X, Coolon R, Ye B. 2013. Dscam expression levels determine presynaptic arbor sizes in Drosophila sensory neurons. Neuron 78:827–838.

Knudson CM, Tung KS, Tourtellotte WG, Brown GA, Korsmeyer SJ. 1995. Bax-deficient mice with lymphoid hyperplasia and male germ cell death. Science 270:96–99.

Koike C, Obara T, Uriu Y, Numata T, Sanuki R, Miyata K, Koyasu T, Ueno S, Funabiki K, Tani A, Ueda H, Kondo M, Mori Y, Tachibana M, Furukawa T. 2010. TRPM1 is a component of the retinal ON bipolar cell transduction channel in the mGluR6 cascade. Proc Natl Acad Sci U S A 107:332–337.

Kuo G, Arnaud L, Kronstad-O'Brien P, Cooper JA. 2005. Absence of Fyn and Src causes a reeler-like phenotype. J Neurosci 25:8578–8586.

Lee SC, Cowgill EJ, Al-Nabulsi A, Quinn EJ, Evans SM, Reese BE. 2011. Homotypic regulation of neuronal morphology and connectivity in the mouse retina. J Neurosci 31: 14126–14133.

Liu G, Li W, Wang L, Kar A, Guan KL, Rao Y, Wu JY. 2009. DSCAM functions as a netrin receptor in commissural axon pathfinding. Proc Natl Acad Sci U S A 106:2951–2956.

Ly A, Nikolaev A, Suresh G, Zheng Y, Tessier-Lavigne M, Stein E. 2008. DSCAM is a netrin receptor that collaborates with DCC in mediating turning responses to netrin-1. Cell 133:1241–1254.

Martinez-Navarrete GC, Angulo A, Martín-Nieto J, Cuenca N. 2008. Gradual morphogenesis of retinal neurons in the peripheral retinal margin of adult monkeys and humans. J Comp Neurol 511:557–580.

Mataruga A, Kremmer E, Müller F. 2007. Type 3a and type 3b OFF cone bipolar cells provide for the alternative rod pathway in the mouse retina. J Comp Neurol 502: 1123–1137.

Matsuoka RL, Nguyen-Ba-Charvet KT, Parray A, Badea TC, Chedotal A, Kolodkin AL. 2011. Transmembrane semaphorin signalling controls laminar stratification in the mammalian retina. Nature 470:259–263.

Matthews BJ, Kim ME, Flanagan JJ, Hattori D, Clemens JC, Zipursky SL, Grueber WB. 2007. Dendrite self-avoidance is controlled by Dscam. Cell 129:593–604.

Milam AH, Dacey DM, Dizhoor AM. 1993. Recoverin immunoreactivity in mammalian cone bipolar cells. Vis Neurosci 10:1–12.

Millard SS, Lu Z, Zipursky SL, Meinertzhagen IA. 2010. Drosophila dscam proteins regulate postsynaptic specificity at multiple-contact synapses. Neuron 67:761–768.

Mosinger Ogilvie J, Deckwerth TL, Knudson CM, Korsmeyer SJ. 1998. Suppression of developmental retinal cell death but not of photoreceptor degeneration in Bax-deficient mice. Invest Ophthalmol Vis Sci 39:1713–1720.

Müller F, Scholten A, Ivanova E, Haverkamp S, Kremmer E, Kaupp UB. 2003. HCN channels are expressed differentially in retinal bipolar cells and concentrated at synaptic terminals. Eur J Neurosci 17:2084–2096.

Nasonkin IO, Lazo K, Hambright D, Brooks M, Fariss R, Swaroop A. 2011. Distinct nuclear localization patterns of DNA methyltransferases in developing and mature mammalian retina. J Comp Neurol 519:1914–1930.

Neves G, Zucker J, Daly M, Chess A. 2004. Stochastic yet biased expression of multiple Dscam splice variants by individual cells. Nat Genet 36:240–246.

Pérez De Sevilla Muller L, Shelley J, Weiler R. 2007. Displaced amacrine cells of the mouse retina. J Comp Neurol 505: 177–189.

Puller C, Haverkamp S. 2011. Cell-type-specific localization of protocadherin beta16 at AMPA and AMPA/kainate receptor-containing synapses in the primate retina. J Comp Neurol 519:467–479.

Reese BE. 2011. Development of the retina and optic pathway. Vision Res 51:613–632.

Rodieck RW. 1991. The density recovery profile: a method for the analysis of points in the plane applicable to retinal studies. Vis Neurosci 6:95–111.

Schmucker D, Chen B. 2009. Dscam and DSCAM: complex genes in simple animals, complex animals yet simple genes. Genes Dev 23:147–156.

Schmucker D, Clemens JC, Shu H, Worby CA, Xiao J, Muda M, Dixon JE, Zipursky SL. 2000. Drosophila Dscam is an axon guidance receptor exhibiting extraordinary molecular diversity. Cell 101:671–684.

Schramm RD, Li S, Harris BS, Rounds RP, Burgess RW, Ytreberg FM, Fuerst PG. 2012. A novel mouse Dscam mutation inhibits localization and shedding of DSCAM. PLoS One 7:e52652.

Soto F, Watkins KL, Johnson RE, Schottler F, Kerschensteiner D. 2013. NGL-2 regulates pathway-specific neurite growth and lamination, synapse formation, and signal transmission in the retina. J Neurosci 33:11949–11959.

Wang J, Zugates CT, Liang IH, Lee CH, Lee T. 2002. Drosophila Dscam is required for divergent segregation of sister branches and suppresses ectopic bifurcation of axons. Neuron 33:559–571.

Wässle H, Riemann HJ. 1978. The mosaic of nerve cells in the mammalian retina. Proc R Soc Lond B Biol Sci 200:441–461.

Wässle H, Puller C, Müller F, Haverkamp S. 2009. Cone contacts, mosaics, and territories of bipolar cells in the mouse retina. J Neurosci 29:106–117.

Wiechmann AF. 1996. Recoverin in cultured human retinoblastoma cells: enhanced expression during morphological differentiation. J Neurochem 67:105–110.

Wikler KC, Stull DL, Reese BE, Johnson PT, Bogenmann E. 1998. Localization of protein kinase C to UV-sensitive photoreceptors in the mouse retina. Vis Neurosci 15: 87–95.

Williams PR, Suzuki SC, Yoshimatsu T, Lawrence OT, Waldron SJ, Parsons MJ, Nonet ML, Wong RO. 2010. In vivo development of outer retinal synapses in the absence of glial contact. J Neurosci 30:11951–11961.

Yamagata M, Sanes JR. 2008. Dscam and Sidekick proteins direct lamina-specific synaptic connections in vertebrate retina. Nature 451:465–469.